PPM1D is a neuroblastoma oncogene and therapeutic target in childhood neural tumors.

Jelena Milosevic[1,2*], Susanne Fransson[3], Miklos Gulyas[4], Gabriel Gallo-Oller[1], Thale K Olsen[1], Diana Treis[1], Malin Wickström[1], Lotta HM Elfman[1], Baldur Sveinbjornsson[1,5], Falk Hertwig[6], Christoph Bartenhagen[7,8], Susanne Reinsbach[3], Margareta Wilhelm[9], Frida Abel[3], Niloufar Javanmardi[3], Subazini Thankaswamy-Kosalai[10], Nina Eissler[1], Anna Kock[1], Yao Shi[11], Keiji Tanino[12], Jane Y Hehir-Kwa[13], Arjen Mensenkamp[14], Godelieve AM Tytgat[13], Chandrasekhar Kanduri[10], Johan Holmberg[11], David Gisselsson[15], Jan J Molenaar[13], Marjolijn Jongmans[13], Matthias Fischer[7,8], Marcel Kool[16,17], Kazuyasu Sakaguchi[18], Ninib Baryawno[1,19], Tommy Martinsson[3], John Inge Johnsen[1,†], Per Kogner[1,*,†,#]

[1]Childhood Cancer Research Unit, Department of Women's and Children's Health, Karolinska Institutet, Stockholm, Sweden.

[2]Center for Regenerative Medicine, Massachusetts General Hospital, Boston, United States.

[3]Department of Laboratory Medicine, Institute of Biomedicine, University of Gothenburg, Gothenburg, Sweden.

[4]Department of Immunology, Genetics and Pathology, Uppsala University, Uppsala, Sweden.

[5]Department of Medical Biology, University of Tromsö, Tromsö, Norway.

[6]Department of Pediatric Oncology and Hematology, Charité-Universitätsmedizin Berlin, Berlin, Germany.

[7]Department of Experimental Pediatric Oncology, University Children's Hospital, Cologne, Germany.

[8]Center for Molecular Medicine (CMMC), Medical Faculty, University of Cologne, Cologne,

Germany.

[9]Department of Microbiology, Cell and Tumor Biology, Karolinska Institutet, Stockholm, Sweden

[10]Department of Medical Genetics and Cell Biology, Institute of Biomedicine, Sahlgrenska Academy, University of Gothenburg, Gothenburg, Sweden.

[11]Department of Cell and Molecular Biology, Karolinska Institutet, Stockholm, Sweden.

[12]Laboratory of Organic Chemistry II, Department of Chemistry, Faculty of Science, Hokkaido University, Sapporo, Japan

[13]Princess Máxima Center for Pediatric Oncology, Utrecht, The Netherlands.

[14]Department of Human Genetics, Radboud University Medical Center, Nijmegen, The Netherlands

[15]Department of Genetics and Pathology, University of Lund, Lund, Sweden.

[16] Hopp Children's Cancer Center (KiTZ), Heidelberg, Germany.

[17]Division of Pediatric Neurooncology, German Cancer Research Center (DKFZ), Heidelberg, Germany.

[18]Laboratory of Biological Chemistry, Department of Chemistry, Faculty of Science, Hokkaido University, Sapporo, Japan.

[19]Department of Stem Cell and Regenerative Biology, Harvard University, Cambridge, USA.

[†]Senior authors with equal contribution

*Correspondence: jelena.milosevic@ki.se (J.M.) and Per.Kogner@ki.se (P.K.)

[#]Lead contact: Per.Kogner@ki.se (P.K.)

48 RUNNING TITLE: *PPM1D* is an oncogene and therapeutic target in cancer

49

KEYWORDS

Neuroblastoma, chromosome 17q, p53, WIP1, *PPM1D*

SUMMARY

Majority of cancers harbor alterations of the tumor suppressor *TP53*. However, childhood cancers, including unfavorable neuroblastoma, often lack *TP53* mutations despite frequent loss of p53 function, suggesting alternative p53 inactivating mechanisms.

Here we show that p53-regulating *PPM1D* at chromosome 17q22.3 is linked to aggressive tumors and poor prognosis in neuroblastoma. We identified that WIP1-phosphatase encoded by *PPM1D*, is activated by frequent segmental 17q-gain further accumulated during clonal evolution, gene-amplifications, gene-fusions or gain-of-function somatic and germline mutations. Pharmacological and genetic manipulation established WIP1 as a druggable target in neuroblastoma. Genome-scale CRISPR-Cas9 screening demonstrated *PPM1D* genetic dependency in *TP53* wild-type neuroblastoma cell lines, and shRNA *PPM1D* knockdown significantly delayed in vivo tumor formation. Establishing a transgenic mouse model overexpressing *PPM1D* showed that these mice develop cancers phenotypically and genetically similar to tumors arising in mice with dysfunctional p53 when subjected to low-dose irradiation. Tumors include T-cell lymphomas harboring *Notch1*-mutations, *Pten*-deletions and p53-accumulation, adenocarcinomas and *PHOX2B*-expressing neuroblastomas establishing *PPM1D* as a *bona fide* oncogene in wtTP53 cancer and childhood neuroblastoma. Pharmacological inhibition of WIP1 suppressed the growth of neural tumors in nude mice proposing WIP1 as a therapeutic target in neural childhood tumors.

INTRODUCTION

Childhood cancers differ from adult malignancies in terms of histopatological entities, biological and clinical features and molecular landscapes[1]. Pediatric tumors are much less complex in their molecular makeup and exhibit significantly less genomic abberations and mutations compared to adult cancers[2]. Despite this, childhood cancer is still the leading cause to death of disease in the developed countries. The tumor suppressor gene *TP53* is the most commonly mutated gene in cancer, and *TP53* mutations are detected in more than 50% of adult cance. Pediatric cancers on the other hand, exhibit significantly less *TP53* mutations[3]. Neuroblastoma, a childhood tumor of the peripheral nervous system exhibits infrequent *TP53* mutations[3]. However, p53 activity is commonly impaired and relapsed tumors demonstrate increased incidence of *TP53* mutations[4]. This suggests that inactivation of p53 is important for tumorigenesis and that alternative mechanisms for p53 attenuation are operating in neuroblastoma.

Segmental gain of chromosome 17q is the most common chromosomal aberration and correlates to poor prognosis in neuroblastoma[5-7]. Located within the gained regions of 17q in high-risk neuroblastoma is the Protein phosphatase magnesium-dependent 1 delta *(PPM1D)* gene which encode the nuclear serine/threonine phosphatase WIP1 (wild-type p53 induced phosphatase 1)[8]. WIP1 is a critical regulator of DNA damage response and cell cycle progression by its ability to regulate the activity of p53, ATM, CHK1/2 and other key molecules involved in DNA repair, cell cycle progression and apoptosis[9-13]. In concordance, *PPM1D* mutations, amplifications and WIP1 overexpression has been observed in various cancers[7,14-21]. This suggest that *PPM1D* is important for tumorigenesis although conclusive evidences for *PPM1D* being an oncogene inducing cancer is still missing.

Here we use multiomic approaches to understand genetic development of neuroblastom focusing on the most common aberration, gain of chromosome 17q, and the oncogenic features of *PPM1D* and p53 regulating WIP1 phosphataseWe show that neuroblastoma patients harbor frequent *PPM1D* copy number gain and gene fusions, in addition to activating truncating germ-line and somatic mutations. We further inferred that overexpression of WIP1 in transgenic mice, in conjunction with cellular stress, induce development of an array of tumors including neuroblastoma, demonstrating that the *PPM1D* is a *de novo* oncogene with the potential to induce tumorgenesis without the support of additional oncogene activities. Finally, we show that WIP1 is a potential clinical therapeutic target in childhood neural tumors.

RESULTS

Chromosome 17q-gain containing *PPM1D* is the most common genetic aberration in neuroblastoma with additional *PPM1D* copies acquired through clonal evolution

To explore the genetic aberrations in neuroblastoma, we used array-based comparative genomic hybridization (CGH) to detect genetic aberrations in 271 Swedish neuroblastomas. Gain of chromosome arm 17q was the most common genetic aberration observed and either segmental 17q gain or whole chromosome 17 gains were present in 82% of the tumors (**Figure S1A**). The majority of unfavorable neuroblastoma, harbored segmental gains of 17q whereas favorable neuroblastomas commonly display whole chromosome 17 gains. Neuroblastoma patients with segmental 17q gain show worse clinical outcome compared to those without 17q gain (5-year overall survival probability 48.0% vs. 82.8%; P=9.8x10^{-9}; **Figure 1A**). The children with favorable neuroblastoma without segmental 17q-gain (or *MYCN* amplification and/or 11q-deletion) had favorable long-term survival at 8-20 years from diagnosis (>90%), in most cases without any treatment, compared to those with 17q-gain receiving active multimodal therapy with risk of late sequelae and still poor survival (<40%; **Figure S1B**), further validating 17q-gain as a prognostic marker.

Our data for the 271 analyzed Swedish neuroblastoma cases (**Figure S1A**) were extended with multiple samples to a total of 435 analyzed samples showed 208 tumors with segmental gain of chromosome 17q. Given the close propinquity to the proximal breakpoints associated with 17q gain and presence in all tumors with segmental 17q gain, the most prominent gene candidates with tumorigenic capacity are *RAD51C*, *PPM1D* and *BRIP1* (**Figure 1B**) out of which only *PPM1D* is a previously proposed putative oncogene (http//:www.cancer.sanger.ac.uk/cosmic/ mutation/).

To further delineate a candidate gene involved in cancer development and to investigate *PPM1D* in neuroblastoma progression, we used evolutionary trajectory analysis[22]. Neuroblastoma copy number status was investigated during tumor progression where we analyzed SNP array data of 100 tumor samples from 23 children with neuroblastoma[22] with focus on chromosome 17. Most tumors (57%, 13/23) were found to harbor gain of 17q (17q+, always including *PPM1D* in the chromosomal gain) in >90% of the tumor cells in all samples, confining this aberration to the stem of evolutionary ideograms, without further change in copy number (**Figures 1C,I and Tables S1**). However, 30% (7/23) of the tumors showed a successive accumulation of 17q copies as tumors evolved regionally or from primary tumor to metastasis or relapse. In four of these cases, *PPM1D*/17q was gained already in the phylogenetic stem, followed by gain of additional copies of these genes as regional clones evolved (**Figure 1C, II**). In three cases, clones with *PPM1D*/17q gain emerged in subset of samples, where they expanded through selective sweeps to encompass all tumor cells in the samples (**Figure 1C, III**). The remaining 13% of patients (3/23) harbored a regionally fluctuating copy number status of *PPM1D*/17q that precluded conclusive evolutionary analysis. Among the 20 cases informative for evolutionary analysis, successive accumulation of *PPM1D*/17q copies was observed in more than half of high-risk patients (7/13) (**Table S1**). In contrast, additional changes in 17q copy number were not found in any of the low-risk patients, i.e. children <18 months with only numerical changes in the stem (0/7; P=0.0445; two-sided Fisher's exact test). Thus, here we identify *PPM1D* as the strongest gene candidate involved in neuroblastoma progression.

In additional neuroblastoma cases with multiple tumor samples available for analysis we show that gain of 17q including *PPM1D* was the single first event in neuroblastoma development (**Fig 1D, Fig S1C** and **S1D)** in both a child without known predisposition and in a child with a germline PHOX2B mutation[23].

To examine if mutations are present in neuroblastoma, we next performed whole exome sequencing (WES) or whole genome sequencing (WGS) of 73 neuroblastoma patient samples to screen for germline and somatic mutations. Notably, we identified a pathogenic truncating *PPM1D* mutation in exon 6 (c.1344_1345insT; p.L450fs) in a *MYCN*-amplified tumor sample obtained from an infant girl with neuroblastoma rapidly progressing after diagnosis from localized INSS stage 1 to metastatic INSS stage 4 (**Figures 1E and S1E**) with fatal clinical outcome despite active therapy. In addition, a *de novo* germline DNA mutation located in exon 6 (c.1528C>T; p.Q510*) resulting in a premature *PPM1D* truncation (**Figure 1E**) was identified in a patient diagnosed with a metastatic (stage 4, INSS/stage M, INRGSS) neuroblastoma of the left adrenal gland with bone metastases. The tumor was diagnosed in a 26 months old boy with history and symptoms similar to those previously reported in children with intellectual disabilities and *PPM1D* germline truncating mutations including significant dysmorphic signs (**Figure S1F**). The tumor had no *MYCN* amplification and the patient had a poor clinical outcome after relapse and progression despite multimodal clinical therapy. A detailed description of this patient is given in Star methods. Germline *PPM1D* mutations have previously not been reported in cancer but have been observed in children with intellectual disabilities and neurodevelopmental disorders[24,25]. Both these neuroblastoma-associated *PPM1D* mutations predictably give rise to C-terminal truncated variants of WIP1 similar to those described in other cancers (**Figure 1E**) (http//:www.cancer.sanger.ac.uk/cosmic/mutation/). In addition, a gene fusion between *PPM1D* and the breast carcinoma amplified sequence 3 *(BCAS3)* gene at chromosome 17q23.2 was identified in a tumor from a patient enrolled in the Therapeutically Applicable Research to Generate Effective Treatments (TARGET) neuroblastoma dataset, which was associated with high expression of *PPM1D* and a predicted WIP1 isoform with a truncated C-terminal (**Figure 1F**).

Overexpression of the *PPM1D* gene in neuroblastoma correlates with unfavorable clinical and biological features

Our data demonstrating that the *PPM1D* gene is altered in copy number and/or structure in the majority of high-risk neuroblastomas, prompted us to investigate the clinical prognostic and biological features of *PPM1D* gene expression in neuroblastoma. First, we show that higher expression levels of *PPM1D* was associated with several neuroblastoma risk factors, i.e. metastatic stage 4 disease, increased age at diagnosis (>18 months), *MYCN*-gene amplification and the INRG high-risk (HR) group as defined by combined clinical and biological features associated with unfavorable clinical outcome[26] (**Figure 2A**). Highest level of *PPM1D* expression was observed in the non-*MYCN* amplified HR-neuroblastoma tumors (nMN HR; **Figure 2A**) mainly corresponding to 11q-deleted tumors that, according the overall genomic landscape, display the most frequent segmental 17q-gain in the *MYCN* non-amplified 11q deleted tumors (**Figure S1A**). Second, quantitative copy number (CN) values for *PPM1D* calculated from CGH array, WES and whole genome sequencing (WGS) was correlated to *PPM1D* expression. CN gains were separated into numerical gains that included whole chromosome 17 and segmental gains that included the sub-region containing *PPM1D*. Correlation analysis revealed a significant stepwise gene dosage dependent expression pattern of *PPM1D,* with the highest expression in tumors with segmental/partial 17q CN gains (**Figures 2A,B**). Moreover, high *PPM1D* expression was related to clinical outcome and children with neuroblastomas showing high expression had worse overall survival (OS; 59% vs. 83% at five years, $p<0.001$, **Figure 2C**, left panel) and event-free survival (EFS; 47% vs. 68%, $p<0.001$, **Figure 2C**, right panel). Third, low-risk neuroblastomas characterized by near-triploid DNA content and high TrkA expression (Type 1)[27] were compared to more aggressive subtypes commonly having 17q gain with 14q- and/or 11q-deletions (Type 2A) or 1p-deletion and *MYCN*-amplification (Type 2B) with principal component analysis (PCA) on gene

expression profiles from 30 primary neuroblastoma samples from two published microarray studies[28,29]. High expression of *PPM1D* was associated with aggressive Type 2A and Type 2B neuroblastomas, while low *PPM1D* expression was observed in Type 1 neuroblastomas (**Figure S2A**). Fourth, immunohistochemical staining showed consistent WIP1 expression in all 17q-gained neuroblastoma samples analyzed (**Figure S2B**). Taken together, these data suggest an increased aggressiveness of neuroblastoma and worse survival for patients with high WIP1-expressing tumors, in line with the predictions of the 17q gain survival data (**Figures 1A and S1B**) and the strong *PPM1D*-17q gain correlation (**Figures 1B,C, 2A,B and S2A**).To extend the investigations on the correlation of chromosome 17 gain and *PPM1D* expression levels, we included medulloblastoma that similar to neuroblastoma also presents frequent chromosome 17q gain or isochromosome 17[3,30] suggesting that there may be a common gene that is involved in the development of both cancers. We analyzed a cohort consisting of 446 human medulloblastoma and 18 normal cerebellum cases and demonstrated that the highest PPM1D/WIP1expression was detected in the clinically unfavorable Group 3 and 4 subgroups (**Figures S2C, Table S2**), that are in line with previous findings[31]. Furthermore, we detected one PPM1D nonsense mutation in exon 6 (E525X; **Figure 1E**) in a medulloblastoma tumor of the WNT subgroup (**Figure S2E**), and amplifications of PPM1D in three patient samples belonging to the clinically unfavorable SHH (4-17 years) subgroup (**Figures S2D and S2F, G**). While, TP53 mutations are significantly associated with the SHH-group and most pronounced to this particular unfavorable SHH subgroup of intermediate ages and adverse outcome[32], neither the PPM1D mutated nor the PPM1D amplified tumors in this analysis had TP53 mutations despite similar age- and prognostic features, indicating an alternative way of impairing p53 function through amplification of PPM1D in these medulloblastoma tumors.

***PPM1D* is important for neuroblastoma development and treatment resistance**

To comprehensively assess the function of *PPM1D*/WIP1 in neuroblastoma as well as in medulloblastoma, we used preclinical models of the diseases. First, we examined the expression of *PPM1D* mRNA in a panel of neuroblastoma and medulloblastoma cell lines, as well as the breast cancer cell lines MCF-7 and BT-474 exhibiting *PPM1D* gene amplification[33], and one sPNET cell line containing isochromosome 17. The cell lines expressed different levels of *PPM1D* mRNA that correlated to their genomic profile[34,35] with highest expression in *PPM1D*-amplified cell lines and lowest in those without chromosome 17 aberrations (**Figures S3A, B**). All neuroblastomas expressed *PPM1D* mRNA, and the highest expression was observed in SK-N-DZ and IMR32, showing expression levels comparable to the *PPM1D*-amplified breast cancer cell lines MCF-7 and BT-474. Furthermore, the relative expression level of *PPM1D* mRNA was higher in medulloblastoma cell lines with 17q-gained aberrations (D283-MED, D458-MED and MEB-MED8A) compared to cell lines with normal 17q (DAOY, UW228-3 and PFSK-1), further demonstrating a gene-dosage effect on *PPM1D* mRNA expression (**Figures S3A, and S3C**).

We next used genome-scale CRISPR-Cas9 screening[36], and demonstrated that *PPM1D* with the highest genetic dependency were found in *TP53* wild-type neuroblastoma cell lines compared to *TP53* mutated cell lines (**Figures 3A and 3B; Supplemental Table S3**). Other *TP53*-negative regulators such as *MDM2*, *MDM4* and *USP7* were ranked as number 3, 21 and 31, respectively. Among the top 40 ranked genes with largest difference between *TP53* wild-type and *TP53* mutated, an enrichment of genes involved in negative regulation of cell proliferation (FDR=0.0117), cell cycle process (FDR=0.0117), cellular response to DNA damage (FDR=0.05) and chromosome organization (FDR=0.05) (**Figure 3C**) was evident.

Focusing on *PPM1D, MDM2, MDM4* and *USP7*, all of which with pharmacological inhibitors that are in preclinical testing or clinical trials, we showed that neuroblastoma cell lines have preferential dependency for all four genes in *TP53* wild-type cell lines (**Figure 3D**). In cell lines of medulloblastoma origin, *MDM2* showed largest difference in dependency score with negative regulators *PPM1D*, *USP7* and *MDM4* ranked 6, 41 and 64, respectively (**Figures S3E and S3H**). Among the top 40 genes there is a functional enrichment of pathways associated to cell cycle (FDR=0.000119), chromosome organization (FDR=0.00065) and nucleotide biosynthesis processes (FDR=0.003) (**Figure S3G**). As expected from the ranked differences between *TP53* wild-type and *TP53* mutated medulloblastomas, only *PPM1D* and *MDM2* showed differences in genetic dependency (**Figure S3H**). When comparing the genetic vulnerability of *PPM1D, MDM2, MDM4* and *USP7* in neuroblastoma cells to all the other cancer cell lines in the CRISPR Avana dataset, both *PPM1D* and *MDM4* showed strong selective dependency in neuroblastoma (**Figure S3D**) highlighting the essentiality of intact p53 (**Figure S3F**).

To study the potential tumorigenic function of *PPM1D*/WIP1 in neuroblastoma we next used genetic manipulation through stable knockdown of short-hairpin RNA (shRNA) against *PPM1D*. The majority of neuroblastoma cell lines transfected with *PPM1D* shRNA were non-viable compared to scrambled controls (data not shown), whereas cells that were viable after transfection showed reduced proliferation and increased H2AX phosphorylation, suggesting an effect on cell viability and genomic integrity (**Figures 3E and S3I**). The multi-resistant neuroblastoma cell line SK-N-BE(2), isolated from a patient with recurrent stage 4 neuroblastoma was chosen for further analysis since this was one of the few cell lines that was viable after *PPM1D* shRNA knockdown (**Figure 3E**). Analyzing different shRNAs constructs directed against *PPM1D* mRNA in SK-N-BE(2) cells established *PPM1D*-shRNA F-1 as the

most effective in reducing *PPM1D* mRNA levels (**Figures 3F,G**). *PPM1D* knockdown was also confirmed by increased phosphorylation of WIP1 target proteins including ATM, CHK1, CHK2, p53 and p38, all involved in cell cycle regulation and the DNA-damage response (DDR) (**Figure 3H**). To test the role of *PPM1D* in cellular stress we subjected SK-N-BE(2) cells to irradiation, and showed that cells lacking *PPM1D* exhibited increased sensitivity to irradiation compared to control cells (**Figure 3I**). Moreover, higher levels of PARP-cleavage were detected in *PPM1D* shRNA transfected cells compared to controls, suggesting an increased vulnerability to apoptosis following irradiation (**Figure 3J**). Furthermore, to evaluate the effect of *PPM1D* knockdown on tumor development *in vivo*, SK-N-BE(2) cells with either *PPM1D*-knockdown or control shRNA were injected subcutaneously in mice and tumor growth was compared. Tumor development was significantly delayed showing median time to tumor development (0.1 mL tumor volume) to be more than doubled (33 days median, vs. 15 days) in the *PPM1D* shRNA knockdown group compared to animals injected with control shRNA-transfected cells ($P<0.001$) (**Figure 3K**).

Mice carrying the *PPM1D* transgene develop tumors in response to cellular stress

Demonstrating that *PPM1D*/WIP1 is a strong gene candidate in the development of neuroblastoma and has a critical function in the growth of tumors and their response to cellular stress, we next investigated the oncogenic potential of *PPM1D*. Hence, we constructed genetically engineered C57BL/6N mice to overexpress WIP1 through pronuclear injection of the human *PPM1D* gene controlled by the rat tyrosine hydroxylase (TH) promoter (**Figure S4A**). Three founder lines were generated with intact transmission of the *PPM1D*-transgene to following generations.

Elevated WIP1 protein expression was detected in spleen, ovary and intestine in mice heterozygous for *PPM1D* compared to wild-type mice (**Figure S4B**). However, no increase in tumor development was observed in these *PPM1D*-transgenic mice. We therefore backcrossed the C57BL/6N*PPM1D* +/- mice for eight generations with 129x1/SvJ mice to establish a near 100% 129x1/SvJ background which is more prone to tumor formation. In addition, given the wide-ranging actions of WIP1 in DNA damage, it is likely that overexpression of WIP under cellular stress has the potential to induce neoplasms arising in response to extrinsic cellular DNA damage. Therefore, *PPM1D*-overexpressing animals and their wild-type littermates were exposed to 4.5 Gy of sub-lethal whole-body irradiation at different ages (1-314 days old). Irradiated transgenic mice carrying the *PPM1D* gene had significantly higher tumor incidence (34% tumor probability) compared to wild-type mice (7.8%) (P<0.0001), 100-300 days post-irradiation (**Figure 4A**). The majority of cancers detected in *PPM1D*- transgenic mice were similar to those reported in irradiated p53-mutant mice post-irradiation[37-39], indicating a similar tumor phenotype caused by p53 impairment rather than p53 absence. Thymic lymphoblastic lymphoma was the most frequently malignancy observed (n=41; **Figures 4B,C**, **Table S4**), compared to four thymic lymphomas detected in irradiated wild-type mice (P<0.001). Other malignancies manifested in *PPM1D*-transgenic mice were leukemia/lymphomas (n=9), different adenocarcinomas/adenomas (n=18) and sarcomas (n=4), (**Table S4**). Importantly, mice also developed neural crest-derived PHOX2B-expressing primary tumors of the adrenal gland with neuroblastoma-like features mixed with paraganglioma/pheochromocytoma-like morphology (one of these mice also displayed PHOX2B-expressing neuroblastoma-like metastasis) (**Figure 4D**), further supporting that *PPM1D* might be a driver of neuroblastoma development. We also identified mice with multiple primary tumors, one mouse with an adenocarcinoma in the lacrimal gland and osteosarcoma with lung metastasis, a mouse with T-cell lymphoma and ovary carcinoma,

lung adenocarcinoma and a mouse with a gastric adenocarcinoma and leukemia (**Table S4**). The odds ratio of developing cancer in mice with the *PPM1D* transgene compared to wild-type mice was 6.3 (95% confidence interval 2.7-14.2). Comparison of age at irradiation and time to tumor development disclosed a positive correlation, showing that younger *PPM1D*-positive animals were more susceptible to developing thymic lymphomas in response to DNA damage ($P<0.01$), the majority (38 out of 41) of which arose <365 days post-irradiation (**Figure 4B**). Protein expression of thymic lymphomas showed high WIP1 expression and increased phosphorylation of p53 compared to non-irradiated thymus from *PPM1D* -positive and wild-type mice (**Figure S4B**). Other tumor manifestations observed in multiple *PPM1D*-positive mice were spleen, liver, lung and lymph node metastases (**Figure S4C and Table S4**).

***PPM1D*-derived mouse tumors show frequent *Notch1* and *Pten* mutations and activation of Notch signaling**

To characterize the tumors that developed in *PPM1D*-transgenic mice, we performed WES on *PPM1D*-derived T-cell lymphomas. Our data showed an average of 18 (range 9-34) somatic protein-changing mutations compared to non-irradiated wild type control mice. Thymic tissues from the two control groups, irradiated wild-type mice, and irradiated *PPM1D*-positive mice without tumors, showed an average of two (range 1-4) and three (range 1-5) somatic protein changing mutation variants, respectively, similar to non-irradiated non-tumorigenic wild type mice (**Table S5**). These data indicate that irradiation alone was not responsible for the accumulation of DNA mutations observed in the tumors. Among the thymic lymphomas, we found *Pten* and *Notch1* to be recurrently altered (**Figure 5**). In total, 15 activating *Notch1* mutations were detected in 9 of 15 lymphomas (60%) and among these, five tumors had more than one mutation of the *Notch1* gene. Similar to human cancers, the *Notch1* missense

352 variants were found to cluster in the heterodimerization domain (HD) while frameshift or
353 nonsense variants were clustered to the proline-glutamic acid-serine-threonine (PEST) domain
354 (**Figure 5A**). Of the 15 sequenced lymphomas, *Pten* aberrations were detected in 12 cases (80
355 %) consisting of homozygous deletions (9 cases), missense variants (2 cases) and frameshift
356 insertion (1 case) (**Figure 5B**). The three missense and frameshift variants all showed high
357 level variant allele fraction (variant allele fraction 85-97%) suggesting a near homozygous
358 presence. Mutations of *Pten* and *Notch1* were co-occurring in seven cases (46%) (**Table S5**).
359 In addition to *Notch1* and *Pten* mutations, aberrations in genes previously associated to
360 human cancers were also observed in *Ikzf1*, *Kras*, *Rac2, Trp53, Ctnnb1*, *Gli3, Zfp36l2, Mpdz,*
361 *Dd3x, Foxp1, Pin1* and *Ezh2* (**Table S5**). No mutations were found in *Fbxw7, Notch2*, *Notch3*
362 or *Notch4* which also have been associated to thymic lymphomas development in radiation-
363 induced murine tumors.
364 We also performed RNA-sequencing on the tumors and analyzed them using Principal
365 component analysis (PCA) and unsupervised hierarchical clustering based on the 200 most
366 variable genes (**Figure S5A, B**). Differential gene expression analysis (**Table S5**) identified
367 4138 upregulated and 4378 downregulated genes in tumors when compared to controls.
368 Tumors harboring *Notch1* mutations had significantly higher expression of the *Notch1* gene
369 compared to controls (**Figure 5C**). Also, as expected *Pten* expression was significantly lower
370 in tumors harboring deletions of the gene (**Figure 5D**). Likewise, gene set enrichment
371 analysis (GSEA) showed corresponding increased expression of genes involved in Notch- and
372 Mtorc1-signalling in *Notch1* or *Pten* mutated tumors compared to controls (**Figure 5E,F**).
373 Thus, tumor development was phenotypically and genetically similar to tumors from p53-
374 impaired mice[38,40] harboring *Notch1*-mutations, *Pten*-deletions and wild-type p53-
375 accumulation.
376

WIP1 is a therapeutic target in neuroblastoma

Having established that *PPM1D*-knockdown reduces tumor formation in mice and that high expression of WIP1 is a strong prognostic factor for poor survival in neuroblastoma, we investigated the effects of compounds inhibiting WIP1 activity in neuroblastoma. To assess the cytotoxic effects of different WIP1 inhibitors on cell viability, six neuroblastoma cell lines and the *PPM1D*-amplified breast cancer cell line MCF-7 were treated with different concentrations of the WIP1 inhibitors SL-176, SP-001 or CCT007093[41-44]. Treatment of neuroblastoma cell lines showed highest sensitivity to the specific WIP1-inhibitor SL-176 regardless of p53 or Mdm2 status. SL-176 displayed the lowest mean of IC_{50} value of the three tested WIP1 inhibitors ($P<0.0001$) (**Figures 6A, S6A and Table S6**).

To further investigate the potency of the WIP1 inhibitor SL-176 on tumor cell viability in monotherapy, a panel of cancer cell lines was treated with different concentrations of SL-176, the p53 modulator RITA, and the MDM2 antagonist Nutlin-3. SL-176 was the most efficient drug against the neuroblastoma cell lines (mean IC_{50} for SL-176: 0.77 µM, RITA: 2.0 µM and Nutlin-3: 3.7 µM), (**Figure 6B, S6C and Table S6**). SL-176 had similar effects on medulloblastoma cell viability as the p53 inhibitors RITA and Nutlin-3. However, no significant differences between the mean IC_{50} values in medulloblastoma cell lines were observed (mean IC_{50} for SL-176: 1.1 µM, RITA: 0.41 µM and Nutlin-3: 3.4 µM, $P=0.26$). The non-cancerous cell lines, MRC-5 derived from human fetal lung fibroblasts and the mouse neural progenitor cell line C17.2 were less sensitive to SL-176 (mean IC_{50} for SL-176: 22 µM, RITA: 9.5 µM and Nutlin-3: 2.0 µM (**Figures S6B, S6C and Table S6**).

Next, we investigated the anti-tumorigenic effect of SL-176 monotherapy in a preclinical *in vivo* model of neuroblastoma Tumor growth inhibition was observed after 1 day of treatment

(SK-N-BE(2); P=0.01) (**Figure 6C**) while tumor size and weight at the end of the experiment was significantly smaller in SL-176-treated mice compared to control mice (SK-N-BE(2); P<0.01, DAOY; P<0.05) (**Figures 6C, D**). No adverse effects of SL-176 were observed in the treatment groups. SL-176 treated tumors showed increase in active caspase-3 and phosphorylation of the DNA repair protein γH2AX, whereas reduced levels of the proliferation marker Ki-67 was observed (**Figure 6E**). Similarly, SL176 also suppressed the growth of established medulloblastoma xenografts in nude mice (DAOY; P=0.02, **Figures S6D, E**) with increased expression of active caspase-3 and γH2AX, and decreased Ki-67 expression (**Figure S6F**). Taken together, our data supports WIP1 as a druggable target in neuroblastoma and medulloblastoma.

DISCUSSION

Neuroblastoma is a childhood tumor of the developing peripheral nervous system, which despite intensified multimodal therapy still have a poor outcome when compared to pediatric cancers in general. For further improvement of management, clinical care and chances of cure for these patients, advancements in molecular understanding of tumor biology is essential. We therefore investigated prevalent genetic aberrations in neuroblastoma as well as for medulloblastoma and our data propose the p53 regulating phosphatase WIP1 encoded by the chromosome 17q-located *PPM1D* gene as a novel druggable target for both these pediatric cancers.

Segmental gain of 17q is the most common chromosomal aberration and predictor of poor prognosis detected in neuroblastoma and medulloblastoma[5,6,45]. Also, gain of chromosome 17q is frequently found in tumors of epithelial, neural and hematopoietic origin[46-51]. This suggests that one or multiple genes important for tumorigenesis are located on 17q. Several cancer-associated genes have been identified on chromosome 17q that besides *PPM1D* also include *EME1, BRCA1, ERBB2, NF1, RAD51C, BRIP1* and *BIRC5*. However, our analysis of 271 Swedish neuroblastoma samples shows that only *RAD51C, PPM1D* and *BRIP1* are included in the shortest region of overlap of 17q gains. These genes were also included in the 17q23.2 chromosomal amplifications detected in three SHH-derived medulloblastomas and are similar to observations made in breast cancer[19,52,53]. We also show an accumulation of *PPM1D* gene copies in metastatic and relapsed neuroblastomas compared to low-risk tumors suggesting a clonal evolution of *PPM1D* in high-risk neuroblastoma. High expression of *BIRC5*, at chromosome 17q25.3, encoding the anti-apoptotic protein Survivin has been correlated with poor prognosis in neuroblastoma, whereas in medulloblastoma conflicting results regarding the importance of Survivin have been reported[54-57]. We detected two somatic

437 *PPM1D* mutations, one each from the neuroblastoma and medulloblastoma cohort and one *de*
438 *novo* germline mutation in one additional neuroblastoma patient. The detected *PPM1D*
439 mutations were all truncating gain-of-function variants and located in exon 6, similar to
440 observations in numerous other malignancies[19,52,53,58]. *PPM1D de novo* germline mutations
441 have previously not been described in cancer. However, in children with intellectual disability
442 syndrome, *PPM1D* germline mutations have been described to occur in the 5th and 6th exons.
443 Notably, an identical c.1528C>T (p.Gln510*) somatic mutation has been reported in a
444 malignant melanoma[59]. The vast majorities of reported somatic *PPM1D* mutationsare located
445 in exon 6 and result in a truncated WIP1 protein with a proposed higher oncogenic capacity
446 compared to the full-length WIP1 protein[19,52,60]. We also detected a gene fusion of *PPM1D*
447 and *BCAS3* in a neuroblastoma patient, predicted to generate a C-terminal truncated WIP1
448 protein and resulting in high levels of WIP1 expression. Similarly, a gene fusion between
449 *PPM1D* and *C1QTNF1* in a Ewing sarcoma patient resulting in high WIP1 expression has
450 been reported (https://pecan.stjude.cloud). Also, a *PPM1D* fusion with an intragenic region of
451 *RPSK6B1* and a *PPM1D-ZNS655* fusion has been reported in a diffuse cerebellar glioma
452 patient and an AML patient, respectively, without any described effects on WIP1 expression
453 (*https://pecan.stjude.cloud)*. Together these observations suggest that the *PPM1D* gene is
454 frequently altered in a variety of cancers and has important functions during tumorigenesis.
455 To functionally test the importance of *PPM1D* in neuroblastoma and medulloblastoma we
456 investigated the effect of genetic or pharmacological inhibition of WIP1 and demonstrated
457 that blocking the expression or activity of WIP1 suppressed both neuroblastoma and
458 medulloblastoma growth *in vivo*. These findings together with similar observations[7,61,62]
459 further support that WIP1 is important for the development and progression of these neural
460 tumors.

WIP1 is a homeostatic regulator of the DNA damage response (DDR) cascade by dephosphorylating and inactivation of ATM, ATR, CHK1, CHK2 and DNA-dependent protein kinase catalytic subunit[63,64]. This and concurrent WIP1-mediated inactivation of p53 will reduce the fidelity of overall DNA repair mechanisms and induce accumulation of DNA aberrations which is a prerequisite for tumorigenesis. Accordingly, we observed increased phosphorylation of DDR proteins and H2AX enhancing the sensitivity to irradiation of *PPM1D* knocked-down neuroblastoma cells. Although mutations of *TP53* are not commonly detected at time of diagnosis in neuroblastoma, the p53 activity is recurrently compromised in these tumors[27,65] and p53 inactivation has been shown to contribute significantly to neuroblastoma development in specific animal models[66,67]. Individuals with the cancer predisposition syndrome Li-Fraumeni caused by germline mutations of *TP53* may occasionally develop medulloblastoma[30,68]. Although uncommon, primary somatic mutations of *TP53* have been linked to the anaplastic medulloblastoma subset[69] and more recently it was shown that *TP53* mutations have subgroup-specific prognostic implications with particular enrichment in the childhood SHH-subset linked to a poor clinical outcome[70]. Furthermore, wild type p53 inactivation in medulloblastoma has been suggested to be related to aberrations in the p53-ARF pathway including *MDM2* and *PPM1D*/WIP1[14,71]. Three of our investigated medulloblastoma samples contained *PPM1D* amplification. All three were detected in the SHH subset in child patients and none had *TP53* mutations, which is frequently observed in this unfavorable subgroup of medulloblastoma[32]. This further validates WIP1 as an important player for tumor development in cancers with impared p53. Also neuroblastoma incidence is increased in Li-Fraumeni families and in particular the specific common p.R337H mutation has been shown to increase neuroblastoma development[72,73].

In primary neuroblastoma, mutations of genes of the p53 pathway are rare, occurring in roughly 5% of the cases[74]. By contrast, *TP53* mutations appear to be more frequent in relapsed neuroblastoma[74] and in neuroblastoma cell lines established at relapse, indicating a role in the development of a therapy resistant phenotype[71,75,76]. Several additional mechanisms for p53 inactivation in neuroblastoma have been described including *MDM2* gene amplification or increased *MDM2* expression mediated by *MYCN* and hypermethylation or deletions of *CDKN2A*, miR-380-5p mediated repression of p53 expression or p53 inactivation by the methyltransferase SETD8[4,77-80]. The demonstration that *Ppm1d*-deficient mice significantly delayed the formation of ERBB2-induced mammary tumors and that *Ppm1d* null embryonic mouse fibroblast were resistant to transformation by RAS, ERBB2 and c-MYC[81] prompted us to establish a genetically modified mouse model overexpressing WIP1. These mice developed tumors of different origin including neuroblastoma after low-dose irradiation compared to wild-type control mice. The spectrum of observed tumors was highly similar to tumors observed in p53 deficient mice or p53 deficient mice receiving irradiation[37-40,82-84]. Interestingly, the tumors developed in our *PPM1D* transgenic mice are phenotypical similar to mice with *Trp53* mutations compared to *Trp53* knockout mice. Mice with *Trp53* deletions mainly develop lymphomas and less frequently sarcomas[38,40] whereas *Trp53* mutant mice, in addition to lymphomas and more frequently sarcoma, also develop carcinomas[39]. This is similar to the spectrum of tumors observed in our *PPM1D* transgenic mice. Thymic lymphoma derived from *PPM1D* transgenic mice expresses high levels of wild-type p53 and WIP1 similar to *Trp53* mutated mice showing high levels of mutated p53[85].

Also, both the genomic landscape and expression profiles obtained from DNA and RNA sequencing of *PPM1D*-induced tumors had similar features with regard to DNA mutations and expression profiles as observed in tumors deriving from p53 impaired mice. Hence,

509 *PPM1D* is an oncogene that induces tumor development by repressing p53 activity leading to
510 deviant cell cycle arrest, DNA repair and apoptosis.
511
512 Taken together, we have dissected the functional role of *PPM1D* in the neural childhood
513 tumors neuroblastoma and demonstrated that *PPM1D* is able to induce tumor growth when
514 cells are subjected to DNA-damaging stress. Hence, *PPM1D* is a *bona fide* oncogene. We also
515 demonstrate that WIP1 constitute a druggable target in neuroblastoma as well as in
516 medulloblastoma that should be further developed and evaluated in combinations with current
517 treatment modalities and investigated for testing in clinical trials given the fact that the
518 majority of patients with poor prognosis have aberrant expression of WIP1. It may be argued
519 that targeting DNA repair mechanisms and phosphatase activity in particular seems a
520 problematic hurdle, but our current data are promising proofs of a principle providing
521 molecular and pharmacological evidence. Furthermore, genetic instability and accumulation
522 of genetic aberrations over time is a major obstacle in metastatic and relapsing pediatric
523 cancers further supporting the potential role and impact of *PPM1D* as a promising therapeutic
524 target for pediatric patients with high-risk neuroblastoma and medulloblastoma as well as a
525 wide range of adult cancer patients.

ACKNOWLEDGEMENTS

We wish to thank Karolinska Center for Transgene Technologies (KCTT) for the transgenic production service. William A. Weiss and Louis Chesler for providing the construct vectors used for generating transgenic *PPM1D*-mice. Clinical Genomics, SciLifeLab, Gothenburg, Sweden and the Bioinformatics Core Facility platforms at the Sahlgrenska Academy, University of Gothenburg, Gothenburg, Sweden for assistance with the bioinformatical analysis of sequencing data. We thank Hjalmar Ståhlberg-Nordegren, Teodora Andonova, Catarina Träger, Inger Bodin and Susanne Ahlberg for their help and contribution to this work. Special thanks to Jessica Lundgren and Selameyhune Assefa for their excellent assistance with the *PPM1D*-transgenic animals. We convey our gratitude to Drs. E Appella and SJ Mazur for useful critical assessment of our manuscript.

This work was supported with grants from the Swedish Childhood Cancer Foundation, the Swedish Research Council, the Swedish Cancer Foundation, the Swedish Foundation for Strategic Research (www.nnbcr.se), Karolinska Institutet, Märta and Gunnar V Philipson Foundation, and The Cancer Research Foundations of Radiumhemmet.

The study sponsors had no role in the design of the study; the collection, analysis, and interpretation of the data; the writing of the manuscript; or the decision to submit the manuscript for publication.

Author contributions. Conceptualization, J.M., J.I.J., and P.K.; Investigation and validation, J.M., S.F., M.G., G.G.O., D.T., M.W., B.S., M.W., L.H.M.E., N.E., A.K., J.Y.H., A.M., G.T.; Computational investigation and analysis, J.M., S.F., T.K.O., F.H., C.B., S.R., F.A., N.J., S. K., Y.S., C.K., J.H., D.G., M.J., M.K., T.M., J.I.J and P.K.; Writing – Original draft, J.M, N.B., J.I.J. and P.K.; Writing – Review & Editing, J.M., S.F., C.K., J.J.M., M.F., M.K., N.B., J.I.J. and P.K.; Resources, K.T., K.S., TM, MF, M.K., J.J.M., G.T., M.J., T.M. and P.K.; Final

551 editing and manuscript approval, All authors; Funding Acquisition & Supervision, J.I.J. and

552 P.K.

553 **Declaration of Interests.** The authors have no conflicts of interest to declare.

554 **STAR METHODS**

555 **Patient-derived tumor material and clinical data**

556 The collection of neuroblastoma (NB) and medulloblastoma (MB) tumors from Swedish
557 patients was performed after either written or verbal consent was obtained from
558 parents/guardians according to ethical permits approved by the local Ethics Committee
559 (Karolinska Institutet and Karolinska University Hospital, registration number 03-736, and
560 2009/1369-31/1(NB), 2009/1608-31/4(MB)). Fresh tumor tissue was obtained at surgery and
561 snap-frozen and stored at -80°C until analysis. Informed consent for using tumor samples in
562 scientific research was provided by parents/guardians of all minors (<18 years of age). In
563 accordance with the approval from the Ethics Committee the informed consent was either
564 written or verbal. Clinical data on all patients were obtained from hospital records and/or the
565 National Solid Tumor Registry (03-736, 03-642, 2009/1608-31/4 and 2009/1369). All patients
566 were diagnosed, managed and treated according to national and international guidelines and
567 protocols.

568

569 **Neuroblastoma patient genomics and transcriptomics**

570 *Patient material for genetic analysis*

571 DNA was extracted from frozen tumors or blood using DNeasy blood and tissue kit (Qiagen,
572 Hilden, Germany) according to manufacturer's protocol and evaluated through absorbance
573 measurements, fluorometric quantitation and DNA integrity assessment on Agilent
574 Tapestation (Agilent, Santa Clara, CA).

575

576 *SNP-microarray analysis*

577 Microarray analysis was performed on a consecutive series of samples from an unselected
578 cohort of 271 neuroblastoma patients using Affymetrix gene mapping arrays (Affymetrix Inc.,

579 Santa Clara, CA). These analyses include the majority of cases from Sweden. All tumors were
580 staged according to the International Neuroblastoma Staging System (INSS) and INRG
581 criteria. Handling of the microarrays has been described previously[6,86].
582 Primary data analysis was performed using GDAS software (Affymetrix) with *in silico*
583 normalization against control samples from healthy individuals with further analyses
584 performed using CNAG (Copy number Analyzer for Affymetrix GeneChip Mapping Arrays)
585 (Genome Laboratory, Tokyo University; http://www.genome.umim.jp). All cases of
586 chromosomal gain, loss, or amplification were scored for both segmental and numerical
587 aberrations, including detailed information about the breakpoint positions when applicable.
588 For practical reasons, all notations of gain and loss were considered in relation to a nominal
589 tumor karyotype and a chromosomal break in a tumor was defined as a clear change in gene
590 dose level in the genomic profile. All genomic position annotations are stated based on the
591 hg19 build (http://genome.ucsc.edu/) of the human genome.
592
593 *Analysis of PPM1D/17q clonal evolution*
594 Single nucleotide polymorphism (SNP) arrays including the Oncoscan (formalin fixed
595 paraffins embedded samples) and Cytoscan HD (fresh frozen samples) platforms (Affymetrix
596 Inc.) were retrieved from and subjected to comparisons of 17q copy number including the
597 *PPM1D* region (pos 17:60,600,183-60,666,280; GRCh38.p12). Evolutionary trajectories were
598 formalized as phylogenetic ideograms along the lines described in the original publication. In
599 all, 100 samples from 23 neuroblastomas from 23 patients were analyzed. Each patient was
600 assigned to one of three simplified clinical-genetic risk groups, including children <18 months
601 with only numerical aberrations found in their tumor's phyologenetic stem by SNP array
602 (low-risk patients), tumors with *MYCN* amplification in the stem (high-risk patients), and
603 tumors with structural rearrangements in the stem (high-risk patients).

Genome sequencing

In total, tumor material from 73 Swedish neuroblastoma patients was subjected to either whole genome and/or whole exome sequencing. Whole exome sequencing was performed through paired-end sequencing on Illumina platforms (Illumina, San Diego, CA) after enrichment with Agilent SureSelect All Exome enrichment kit (Agilent technologies, Santa Clara, CA) on DNA for 18 tumor/normal pairs and additional 20 neuroblastoma tumors without corresponding constitutional DNA. Alignment against hg19 was performed using BWA with GATK local realignment followed by SNV calling using SNPeff. Whole genome sequencing (WGS) was performed on tumor DNA and corresponding constitutional DNA extracted from blood for 35 neuroblastoma patients for an average coverage of at least 60X for tumor and 30X for constitutional DNA using Illumina xTen instrumentation (Illumina, San Diego, CA, USA) located at NGI/Clinical Genomics, SciLife Laboratories, Stockholm, Sweden. Read trimming, mapping to the human reference genome hg19 and variant calling were performed using CLC Genomics Workbench 8.0.3 software (CLC, Aahus, Denmark). Only high quality called variants with a minimum 10% allele frequency and a total read coverage of ten were considered for further analysis. Somatic variants with allele frequency above 3% in either 1000 genomes, Exome Aggregation Consortium (ExAC), Cambridge, MA (http://exac.broadinstitute.org) or NHLBI Exome Sequencing Project (http://evs.gs.washington.edu/EVS/) were discarded as well as excluding all synonymous variants or variants in non-coding regions except those affecting canonical splice sites. Remaining variants were assessed manually through the Integrative Genomics Viewer (IGV)[87] for removal of calls due to mapping artifacts and paralogs.

For tumors (exome) sequenced without corresponding DNA from constitutional tissue, a systematic filtering approach was used to identify critical variants. This was done by removal

of common variants, e.g. present in dbSNP v138 or showing an allele frequency above 0.1 in either 1000 genomes, Exome Aggregation Consortium (ExAC), Cambridge, MA (http://exac.broadinstitute.org), NHLBI Exome Sequencing Project (http://evs.gs.washington.edu/EVS/) or SweFreq (https://swegen-exac.nbis.se/). Variants were annotated based on RefSeq and functional impact was predicted by SIFT and PolyPhen. FusionCatcher was applied to discover *PPM1D*-containing fusion transcripts in the National Cancer Institute TARGET dataset comprising paired-end RNA sequenced neuroblastoma patient samples (dbGap Study Accession:phs000218.v16.p6).

Case description, germline PPM1D mutation detection

The patient was born by a spontaneous delivery at gestational week 37+4 after an uneventful pregnancy. His birth weight was 2945 gr. He was diagnosed with a bicuspid aortic valve, which was also present in the maternal grandmother and two of her siblings. The family history was negative for cancer with onset before age 50. In the first year of life he had reflux for which feed thickener and proton pomp inhibitors were described. Psychomotor development was above average with early speech development, early recognition of numbers, letters and colors and walking shortly after his first birthday. At 26 months of age he presented with hemifacial paresis and clinical, radiological and pathological evaluation revealed a metastatic stage 4 (INSS) intermixed ganglioneuroblastoma of the left adrenal gland with bone metastases in the skull base, in the lumbosacral spine with intraspinal extension and expansion to the left-sided ilium and diffuse bone marrow infiltration. The tumor was negative for *MYCN* amplification and negative for LOH of chromosome 1p. Therapy consisted of induction chemotherapy, surgical resection, high dose chemotherapy, autologous stem cell transplantation and radiotherapy which resulted in very good partial clinical remission. Treatment was intended to be completed with immune therapy but

654 evaluation before starting this treatment revealed refractory neuroblastoma in the ilac bone,
655 which was irradiated and again three cycles of chemotherapy (irinotecan/temozolomide) were
656 given. The evaluation that followed showed diffuse leptomeningeal metastases indicative of
657 progressive disease. Palliative treatment was started and the boy died at 3 years and 7 months
658 of age. During treatment it was noted that the boy had a remarkably high pain threshold.
659 Shortly after his cancer diagnosis the parents worried about a possible increased risk for
660 neuroblastoma in the younger brother of the proband and a clinical geneticist was consulted.
661 Fetal fingers pads and a relatively short stature (at cancer diagnosis his age-adjusted length
662 and head circumference were at -1.5 SD) were observed in the proband, but otherwise no
663 dysmorphisms or other notable features were present. Germline *PHOX2B* and *ALK* analysis
664 revealed no mutations. Several years later, the brother developed subcutaneous lesions on his
665 right forearm at three years of age. These were resected and were hard to classify by the
666 pathologist, with benign myofibroblastic proliferation as most likely diagnosis. The parents
667 again consulted a clinical geneticist, in the light of a possible genetic predisposition
668 explaining the tumors in their children. Whole exome sequencing was performed on blood
669 derived DNA of both children and the parents. This revealed a heterozygous c.1528C>T
670 (p.Gln510*) mutation in *PPM1D* in the proband who died of neuroblastoma. This mutation
671 was absent in his brother and his parents. Identification of this mutation in neuroblastoma
672 derived DNA confirmed the germline status of this mutation and excluded that the mutation
673 was restricted to blood and resulted from chemotherapy which has recently been shown for
674 *PPM1D* mutations[88].
675
676 The patient described here has several features in overlap with patients with *PPM1D*
677 intellectual disability syndrome. He had relative short stature, reflux in early childhood, small
678 hands (hand length -2,5 SD at age 9 months), and a high pain threshold. Strikingly,

679 developmental delay was definitely absent in this child. Despite intensive multimodal
680 treatment for his high-risk neuroblastoma, he seemed to have an above average intelligence,
681 which was in concordance with the education levels of his parents and grand parents.
682 Additionally, deep phenotyping revealed overlapping behavioral problems (ASD, ADHD, and
683 anxiety disorders), hypotonia, broad-based gait, facial dysmorphisms, and periods of fever
684 and vomiting. This patient, with the first de novo germ-line *PPM1D* mutation linked to
685 cancer, showed a facial phenotype that significantly correlated (p=0.0164, **Supp Figure S1F**)
686 with eleven previous reported patients with de novo germ-line truncating *PPM1D* mutations
687 of the 5th or 6th exon and intellectual disability[24].
688
689 *Gene expression analysis*
690 Patient cohort and methodology of RNA-seq data analysis pipeline are extensively described
691 in[89]. We used gene expression data of 498 neuroblastoma patients from seven countries.
692 According to the Neuroblastoma Risk Group (INRG) classification system[26] we classified
693 patients with *MYCN* amplifications and patients with a metastatic disease and older than 18
694 months at diagnosis as high-risk patients (n=176). Events were defined according to a revised
695 version of the International Neuroblastoma Response Criteria[90].
696 RNA-seq gene expression analyses have been done using the MAGIC-AceView pipeline as
697 previously described[89]. Copy number data for *PPM1D* was derived from array comparative
698 hybridization (aCGH);[91], whole exome sequencing and whole genome sequencing analyses[74].
699
700 *Statistical analyses*
701 Gene expression of *PPM1D* was investigated displayed on the gene level (*PPM1D*) or
702 transcript level for two selected transcript variants (AceView annotation, as a result of the

703 analysis, i.e. *PPM1D.aAug10* and *PPM1D.bAug10*, corresponding to transcripts
704 ENST00000305921 and ENST00000392995 respectively).
705 *PPM1D* expression in defined NB subgroups (according to INRG high-risk status, INSS
706 stage, amplification status of MYCN, age, CN status of *PPM1D* on chromosome 17) was
707 displayed in Tukey box-and-whisker plots (box range: inter-quartile range, whiskers: 1.5x
708 IQR). Where appropriate, either Mann–Whitney–Wilcoxon or Kruskal-Wallis tests were
709 performed to investigate differences in expression of two or more analyzed groups,
710 respectively. Pearson correlation analyses have been applied to investigate correlation
711 between *PPM1D* expression and copy number.
712
713 To investigate the prognostic value of *PPM1D* expression, optimal cutpoint expression values
714 separating the cohort into *PPM1D*-high and *PPM1D*-low groups that correlate best with
715 outcome in terms of event-free survival (EFS; recurrence, progression and death from disease
716 were considered as events), and overall-survival (OS) were calculated by means of maximally
717 selected rank statistics (maxstat package in R v3.4.3)[92,93] in training sets. Differences in
718 survival of *PPM1D* high and low-expressing subgroups according to dichotomization with the
719 established cutpoints was then tested by Mantel-Cox (log-rank) tests in corresponding
720 validation sets. For this procedure, equally sized training and validation subsets (n=296) were
721 randomly sampled from the entire cohort (n=498). Resampling was done 1000 times and the
722 mode of those established cutpoint values which passed $p < 0.05$ in maxstat[92,93] as well as in
723 the log-rank test was eventually selected to define *PPM1D*-high and *PPM1D*-low expressing
724 subgroups (this procedure was independently done for EFS and OS). Subsequently, Kaplan-
725 Meier survival estimates for the entire cohort were calculated and displayed from the time of
726 diagnosis and clinical outcome of respective subgroups was compared using the log-rank test.
727

Principal Components Analysis (PCA) on expression data

Raw data expression: CEL-files (HU133A chips from Affymetrix) from 30 primary neuroblastoma cases from two published microarray studies[28,29,94] were pre-processed using gcRMA normalization in Bioconducter for R 2.9.2 (library BioC 2.4). For each gene, the mean expression level from probe-sets was calculated, resulting in 8105 genes/variables[94]. Principal Components Analysis (PCA) was performed on the pre-processed McArdle/Wilzén expression data set using Omics Explorer 3.2 from Qlucore (www.qlucore.se). Genes with the lowest variance were filtered out (variance cut-off =0.4), displaying a PCA plot based on 716 genes/variables and 30 samples/cases according to the method previously described[94]. Samples/cases were joined to their nearest neighbor using Euclidean distances, and they subdivided into four separate groups. The differential expression of *PPM1D* between molecular subgroups was calculated by fold change and change and Student's t-test (2-sided comparison, unequal variance).

Gene expression data profiling for medulloblastoma

All mRNA expression data of 446 human medulloblastoma and 18 normal cerebellum samples have been generated by Affymetrix U133plus2.0 arrays. Gene expression data come from public sources deposited in GEO (http://www.ncbi.nlm.nih.gov/geo)[95-99] or have been generated at the German Cancer Research Center DKFZ in Heidelberg. The MAS5.0 algorithm of the GCOS program (Affymetrix Inc) was used for normalization of the expression data. All data have been analyzed using the R2 program for analysis and visualization of microarray data (http://R2.amc.nl). Anova tests were used to test whether there is a significant differential expression of WIP1 between the groups shown in the plots.

Cell culture and reagents

753 Twenty-two human cell lines of different origin were used throughout the study: eleven
754 neuroblastoma cell lines (IMR-32, Kelly, NB1691, SH-EP, SH-SY5Y, SK-N-AS, SK-N-
755 BE(2), SK-N-DZ, SK-N-FI, SK-N-SH, TR14), eight medulloblastoma/sPNET cell lines
756 (DAOY, D283MED, D384MED, D425MED, D458MED, MEB-MED8A, PFSK-1, UW228-
757 3), two breast cancer cell lines (MCF-7, BT-474), and one human fetal lung fibroblast cell
758 line (MRC-5). In addition, one neural multipotent progenitor cell line from mouse (C17.2)
759 was used. The cell lines were purchased from ATCC, except D384MED, D425MED,
760 D458MED, PFSK-1, MEB-MED8A and UW228-3 that were kindly provided by Dr. M.
761 Nistér (Karolinska Institutet), NB1691 and TR14 by Dr. D. Tweddle (Newcastle University)
762 and C17.2 by Dr. T. Ringstedt (Karolinska Institutet). The cell lines were cultured in RPMI
763 1640 (IMR-32, Kelly, NB1691, SH-EP, SK-N-AS, SK-N-BE(2), SK-N-DZ, SK-N-FI, SK-N-
764 SH, TR14, PFSK-1 and MRC-5), Dulbecco's modified Eagle's medium (DMEM; MEB-
765 MED8A, C17.2, BT-474), Minimum Essential Media (MEM; DAOY, D283MED,
766 D384MED), Richter's improved MEM with zinc/DMEM (IMEMZO/DMEM; D425MED and
767 D458MED), DMEM/F12 (SH-SY5Y and UW228-3). Medium was supplemented with 10%
768 (or 15% for C17.2, MEB-MED8A, D425MED and 20% for D384MED) heat-inactivated fetal
769 bovine serum (FBS), 2 mM L-glutamine, 100 IU/ml penicillin G, and 100 µg/ml streptomycin
770 (Life Technologies Inc., Stockholm, Sweden) at 37°C in a humidified 5% CO_2 atmosphere.
771 To the MCF-7 and D384MED media, 1 mM sodium pyruvate and 1 mM non-essential amino
772 acids solution (Gibco) were also added. All media were purchased from Gibco BRL.
773
774 The identities of the cell lines were verified by short tandem repeat genetic profiling using the
775 AmpFlSTR® IdentifilerTM PCR Amplification Kit (Applied Biosystems) in December 2015
776 and all cell lines were used in passages below 25. All experiments were executed in Opti-
777 MEM (GIBCO) supplemented with glutamine, streptomycin and penicillin (HyClone Thermo

778 Fisher Scientific), except transfection experiments, which were performed without antibiotics.
779 *PPM1D*-knockdown SK-N-BE(2) cells and corresponding control cells were cultured in
780 selection media (standard media according to above supplemented with 0,5-2 µg/mL
781 puromycin).
782
783 RITA and Nutlin-3 were purchased from Cayman Chemical Company and Sigma-Aldrich,
784 respectively, and SL-176 and SPI-001 were synthesized as described previously[42,44]. RITA
785 and Nutlin-3 were dissolved in DMSO (Sigma-Aldrich), while SL-176 was dissolved in a mix
786 of DMSO (33%) and ethanol (67%). Further dilutions were made in Opti-MEM or PBS. The
787 DMSO concentration did not exceed 1% v/v in any experiment. For the *in vivo* studies, SL-
788 176 was dissolved in a mix of DMSO (33%) and ethanol (67%) and further diluted in sodium
789 chloride 0.9%.
790
791 **Short hairpin RNA (shRNA)**
792 For the transfections, cells were seeded in 6-well plates, left to attach and transfected using
793 Lipofectamine 2000 (Thermo Fisher Scientific) with 4 µg of four pre-designed shRNAs
794 (GIPZ Lentiviral) targeting human *PPM1D* (172_0502-F-1 (Clone ID: V2LHS_262759),
795 172_0556-D-7 (Clone ID: V2LHS_27794), 172-0447-C-2 (Clone ID: V2LHS_27798) and
796 172_0496-G-2 (Clone ID: V2LHS_262763), Dharmacon) and non-silencing pGIPZ Lenti
797 Control shRNA (#RHS4346, Dharmacon). Cells were incubated for 6 hours in the
798 transfection media and then replaced with corresponding culture medium. After 24-48 hours,
799 cells were subjected to further analyses. For generating stable transfections, cells were grown
800 in selective medium (0,5-2 µg/mL puromycin selection).
801
802 **Viability assays**

For evaluation of cytotoxic effect on cell viability, we used the fluorometric microculture cytotoxicity assay as previously described[100] or the colorimetric formazan-based assay WST-1 (Roche), according to the manufacturer's description. Briefly, cells were seeded into 96 well plates (5 000 – 10 000 cells/well), left over night and treated with drugs the following day. After 72 hours, WST-1 reagent was added and absorbance was measured at 450 nm. All concentrations were tested in triplicate. The mean out of at least three independent experiments is reported.

To determine colony formation, 100 cells/well in the non-exposure experiments and 300 cell/well in the irradiation experiments were seeded in 60 mm cell+ culture plates (Sarstedt, Sweden) and allowed to attach for 24 h before exposure to ionizing radiation (Cobolt^{60} source) at 2 or 4 Gy, when applicable. After 10-14 days of incubation in medium, cells were washed, fixed in formaldehyde (4%), stained with Giemsa (Gibco, BRL) and colonies (1 clone>50 cells) with 50% plate efficiency were manually counted. The mean out of at least three experiments is reported.

Cell viability of *PPM1D* silencing was assessed by the trypan blue exclusion assay. In brief, cells (4.4 x 10^4 MEB-MED8A cells/well and 2.5 x 10^4 SK-N-BE(2) cells/well respectively), were seeded and transfected in 6-well plates; 3 wells for each time point per cell line and transfection group, cultured for 6 days. Cells were stained with 0.4% trypan blue (GIBCO, BRL) and viable (unstained) cells were counted daily to determine the total number of living cells. The mean out of three experiments is reported.

Irradiation of human cancer cell lines

SK-N-BE(2), SH-SY5Y, DAOY, Med8a and MCF-7 cells were seeded into six-well cell culture plates (300 000 – 500 000 cells/well) in standard medium with 10% FBS and allowed

to attach overnight, with exception for Med8a cells growing in suspension. Prior to treatment, 60-80% confluency was observed. Medium was removed and replaced with OptiMEM containing a SL-176 concentration equivalent to the corresponding IC_{50} value for each cell line (0.5 - 1.3 µM). Med8a cells were directly seeded in OptiMEM containing SL-176 at IC_{50}. After 1h incubation, cells were irradiated with 4 Gy ($Cobolt^{60}$ source) while kept on ice, after which incubation at 37°C continued for the time indicated (0, 4, 8, or 24 hours). Cells were harvested using Cell Dissociation Solution Non-enzymatic (Sigma-Aldrich). For the irradiation of the stably transfected SK-N-BE(2) neuroblastoma cell lines (*PPM1D* ShRNA and control ShRNA), 500 000 cells/well were seeded into six-well cell culture plates as described above, allowed to attach overnight and irradiated with 2 Gy and 4 Gy respectively and harvested after 48 and 72 hours. SK-N-BE(2) non-transfected cells were treated with 40mM cisplatin, used as a positive control for double-strand DNA breaks.

Western blot

Protein extraction, determination of protein content, SDS-PAGE under reducing conditions, electroblot and immunoreaction detection were carried out as previously described[101]. Briefly, total proteins were extracted using RIPA buffer (Thermo Fisher Scientific) supplemented with Halt™ Protease and Phosphatase Inhibitor Cocktail (Thermo Fisher Scientific). 30 µg (for cell lines) and 50 ug (for mouse tissue) of total protein were resolved by reducing SDS-PAGE and transferred onto a nitrocellulose membrane. The membranes were blocked with 5% non-fat milk or BSA 5% in TBS-T buffer, and incubated with the corresponding antibodies (**Table S7**). Chemiluminescence visualization of antibodies was performed with Amersham™ ECL™ Prime Western Blotting Detection Reagent (GE Healthcare). Visualization and imaging of signal was performed with ImageQuant LAS 4000 (GE Helathcare).

853 **Quantitative real-time RT-PCR analyses**

854 The mRNA expression levels were quantified using TaqMan® technology on an ABI PRISM
855 7500 sequence detection systems (PE Applied Biosystems). Primers were selected from the
856 Assay-on-Demand products (Applied Biosystems), including human *PPM1D*
857 (Hs00186230_m1), and 18S ribosomal RNA (Hs99999901_s1). All gene expression assays
858 was designed with an FAM reporter dye at the 5' end of the TaqMan MGB probe, and a non-
859 fluorescent quencher at the 3' end of the probe. High capacity RNA-to-cDNA kit (Applied
860 Biosystems) was used to synthesize cDNA from 100 ng of RNA per sample. The PCR
861 reaction was done in a total reaction volume of 25 µl containing 1 x TaqMan® Universal PCR
862 Master Mix, 1 x TaqMan® Gene Expression Assays (Applied Biosystems) and 10 µl of
863 cDNA from each sample as a template, in MicroAmp optical 96-well plates covered with
864 MicroAmp optical caps (Applied Biosystems). Firstly, samples were heated for 2 min at 50°C
865 and then amplified for 40 cycles of 15 s at 95°C and 1 min at 60°C. A standard curve was
866 generated for relative quantification with cDNA synthesized from 1 µg RNA of the cell lines
867 combined. For every sample the amount of target mRNA was normalized to the standard
868 curve and normalized to 18S ribosomal RNA expression. All experiments included a no
869 template control and were performed in triplicate.
870
871 **CRISPR-Cas9 loss of function screening**
872 The DepMap Public CRISPR (Avana) 18Q3 gene dependency dataset including 485 cancer
873 cell lines (whereof 15 neuroblastom and 7 medulloblastoma cell lines) as well as mutation call
874 dataset was downloaded from the Broad Institute Cancer Dependency Map
875 (https://depmap.org/portal/) and used for analysis of *PPM1D* and *TP53* genetic
876 vulnerabilities[102]. Visualization and analysis of enriched functional processes associated to

TP53-dependency was done in the Search Tool for the Retrieval of Interacting Genes/Protein (STRING) database[103].

Flow cytometry

Phosphorylation of H2AX was assayed with Alexa Fluor 647-conjugated anti-phospho-H2AX (2F3, Biolegend, San Diego, CA, USA) 24 and 72 hours on cells that were transfected with *PPM1D*-shRNA 172_0502-F-1 and control shRNA, respectively. A minimum of 10 000 events were recorded on Becton-Dickinson FACSCalibur or LSR II flow cytometers (BD Biosciences, San Jose, CA, USA). Data analysis was performed using the Cell Quest software.

Human tissue samples for immunohistochemistry

Neuroblastoma and medulloblastoma tumor tissue were obtained from the Karolinska University Hospital according to the ethical approval from the Stockholm Regional Ethical Review Board and the Karolinska University Hospital Research Ethics Committee (approval ID 2009/1369-31/1 and 03-736). Informed consent (written or verbal) was provided by the parents or guardians for the use of tumor samples in research. Samples were collected during surgery, snap-frozen in liquid nitrogen and stored at -80°C until further use. Twenty-seven neuroblastoma samples derived from children of different ages and all clinical stages, including different biological subsets[104], were analyzed.

Immunohistochemistry

Formalin-fixed and paraffin-embedded human tissue sections were deparaffinized in xylene and graded alcohols, hydrated and washed in phosphate-buffered saline (PBS).

After antigen retrieval in sodium citrate buffer (pH 6) in a microwave oven, the endogenous peroxidase was blocked by 0.3 % H2O2 for 15 min. Sections from human neuroblastoma were incubated overnight at 4 °C with a primary antibody against PPM1D (ab31270, Abcam). Similarly, tissue sections from xenograft tumors were incubated with an anti-Ki-67 antibody (clone SP6, Neomarkers, Fremont), anti-cleaved caspase-3 (ASP175) (#9579; Cell Signaling Technology) and anti phospho-Histone h2ax (Ser139) (#9718 Cell Signaling Technology), respectively. As a secondary antibody, the anti-rabbit-horseradish peroxidase (HRP) SignalStain Boost IHC detection kit was used (Cell Signal Technology; #8114). A matched isotype control was used as a control for nonspecific background staining (not shown).

Animal studies

Ethical permits

The animal experiments were approved by the regional ethics committee for animal research in Northern Stockholm, appointed and under the control of the Swedish Board of Agriculture and the Swedish Court. All animal experiments were in accordance with national regulations (SFS 1988:534, SFS 1988:539, and SFS 1988:541). For specific approval numbers, please refer to the sections below.

Xenograft studies

Immunodeficient nude mice (female 4-6 weeks old, NMRI-nu/nu, Scanbur, Stockholm, Sweden) were used for xenograft studies (ethical approvals N304/08 and N391/11). The mice were kept under specific pathogen-free conditions at a maximum of six individuals per cage and given sterile water and food *ad libitum*. All mice were treatment-naïve at the start of the experiment.

926 Under general anesthesia, each mouse was injected subcutaneously on the rear flank with 10 x
927 10^6 SK-N-BE(2) neuroblastoma cells or 17 x 10^6 DAOY medulloblastoma cells. In the
928 knockdown experiment, mice were inoculated bilaterally with 5 x 10^6 SK-N-BE(2) cells
929 (clone d) that were knocked down for *PPM1D* (n=8) and SK-N-BE(2) control cells (clone C)
930 that were transfected with non-silencing shRNA (n=15) respectively and followed until the
931 tumor reached 0.1 mL.
932 In the drug treatment experiments, mice with SK-N-BE(2) xenografts were randomly
933 assigned to three different treatment groups when the tumor reached ≥0.1 mL. For twelve
934 days, mice received either daily intraperitoneal injections (i. p.) of SL-176 at 3 mg/kg (n=8) or
935 0.5 mg/kg (n=6), or no treatment (n=6). The mean tumor volume at the start of treatment was
936 0.115 mL.
937 Mice bearing DAOY xenografts were randomly divided into two different groups, and
938 treatment commenced at tumor volume ≥0.12 mL. Mice received either 3 mg/kg SL-176 as
939 daily i. p. injection for 21 days (n=8), or no treatment (n=7). The mean tumor volume at the
940 start of treatment was 0.124 mL.
941 In all xenograft-bearing mice, tumors were measured every day and the animals were
942 monitored for signs of toxicity including weight loss. The tumor volume was estimated as
943 $(\text{width})^2$ x length x 0.44. At sacrifice, tumors were dissected and either frozen or fixed in
944 formaldehyde, for subsequent analyses.
945
946 *WIP1-overexpressing mouse model*
947 Transgenic WIP1-overexpressing mice were generated by pronuclear injection with random
948 integration of a *PPM1D*-transgenic vector construct, carried out at Karolinska Center for
949 Transgene Technologies (KCTT) and granted according to ethical approval numbers N251-12
950 and N42-14.

951 The construct consisted of rat tyrosine hydroxylase (TH) promoter, meant to direct expression
952 towards the neural crest; rabbit beta-globin intron was used to enhance expression; and cDNA
953 for the human *PPM1D* gene. Herpes simplex virus (HSV) thymidine kinase gene sequence
954 was used as a transcription terminator (**Figure S4A**). The plasmid was kindly provided by
955 Prof. William Weiss (University of California, San Francisco, California, USA) and has
956 previously been used to generate a transgenic mouse model with targeted *MYCN* expression
957 giving rise to murine neuroblastoma[67]. In the current study, however, *MYCN* cDNA was
958 substituted for *PPM1D* cDNA (MGC Human *PPM1D* Sequence-Verified cDNA, Clone Id:
959 5167004, Dharmacon) to complete the construct (GENEWIZ, South Plainfield, NJ, USA).
960
961 The linearized and purified construct was diluted to 1.5 ng/ul in microinjection buffer (10 mM
962 Tris-HCl, pH7.4, 0.1 mM EDTA) and injected into the pronucleus of C57BL/6NCrl zygotes
963 using a Nikon TE200 microinjection system with Narishige NT-88NEN micromanipulators
964 and a Warner Instruments PLI-100A pico-liter injector. The microinjected embryos were
965 transferred into the oviducts of pseudopregnant Crl:CD1(ICR) female mice using standard
966 surgery techniques and ear biopsies from the resulting 55 offspring were screened for the
967 presence of the *PPM1D* transgene by PCR using
968 forward primer: 5′-CTGGTCATCATCCTGCCTTTCT-3′ and
969 reverse primer: 5′-GCCTTTCCCCGAGACTTCG-3′ (Sigma-Aldrich). 6 transgenic animals
970 were found of which 4 founder animals were further established based on their ability to pass
971 on the human *PPM1D*-transgene to their offspring.
972
973 In order to achieve a more tumor-permissive genetic background, these four transgenic
974 mouse-lines were backcrossed with 129X1/SvJ mice, aiming for ten generations of
975 backcrossing which should result in approximately 100% 129X1/SvJ background.

Backcrossing was carried out in accordance with ethical permit number N641-12. Throughout breeding, mice were monitored closely for development of palpable abdominal tumors or other disease manifestations up to 548 days (1.5 years) of age.

Irradiation of mice

Using a linear accelerator (X-RAD 320, Biological Irradiator, North Branford, CT, USA) with a dose rate of 0.95 Gy/min at 320 KV and a radiation field of 20 x 20 cm, *PPM1D*-transgenic mice from three established transgenic lines and their wild-type littermates resulting from heterozygous breeding pairs with different degrees of 129X1/SvJ strain background (3 to 7 generations of backcrossing from C57BL/6N to 129X1/SvJ background) were subjected to whole-body irradiation at a single sublethal dose of 4.5 Gy (ethical approval N290-15), after which they were monitored daily in their usual pathogen-free environment. Mice were exposed to irradiation at different ages (1 to 314 days old). Littermates were always irradiated simultaneously. The mice were followed up to 548 days (1.5 years) of age.

Immunohistochemistry of transgenic mouse tissue samples

Formalin-fixed and paraffin-embedded transgenic mouse tissue sections were deparaffinized in xylene and graded alcohols, hydrated and washed in phosphate-buffered saline (PBS). After antigen retrieval in sodium citrate buffer (pH 6) in a microwave oven, endogenous peroxidase activity blocked by 0.3 % H_2O_2 for 15 min. Biotin blocking was preformed using an avidin/biotin blocking kit (Vector Laboratories). All washes and dilutions were performed in PBS containing 0.1% saponin. Sections were incubated with an anti-Ki-67 antibody (clone SP6, ab16668, abcam), anti-B220 antibody (clone RA3-6B2, R&D Systems, Minneapolis, MN, USA), or anti-CD3 antibody (SP7, Abcam, Cambridge, UK) containing 3% human serum overnight at room temperature. After blocking with 1% goat serum for 15 min sections

were incubated with a biotin-conjugated secondary antibody (goat anti-rabbit IgG or goat anti rat IgG, Vector laboratories) containing 1%goat and 3% human serum at room temperature for 30 min. For detection an ABC complex (Elite ABC kit, Vector laboratories) was used before the sections were developed using diaminobenzidine (DAB Peroxidase Substrate kit; Vector Laboratories) as chromogen. Sections were counterstained with Mayer´s hematoxylin (Histolab). For immunofluorescence detection of CD3 positive cells sections were incubated with anti-CD3 antibody (SP7, Abcam, Cambridge, UK) in 4% goat serum overnight at +4C following incubation with secondary Goat anti-rabbit-Alexa Fluor 488 (Thermo fisher Scientific). Histological assessment of the transgenic mouse tissues was performed by a pathologist. For full list of antibodies used for immunohistological analyses see **Table S7**.

Whole exome sequencing, variant calling and copy number alterations in mice

Whole exome sequencing (WES) was performed on DNA from totally 24 samples; 15 independently developed thymic lymphomas and thymus from nine controls. The controls were dived in to three different groups corresponding to a) irradiated *PPM1D*-transgenes, b) irradiated wild type and c) non-irradiated wild type. In respective control group three mice, one from each strain, were subjects for sequencing.

WES was performed by Otogenetics (Otogenetics Corporation, Atlanta, GA, USA) through pair-end sequencing on Illumina platforms (Illumina, San Diego, CA) after enrichment with Agilent SureSelectXT Mouse All Exon (Agilent technologies, Santa Clara, CA) reaching an average coverage of 80X (range 47,5-99,2X) (**Table S5**). Read trimming, mapping to the mouse reference genome mm10 and variant calling were performed using CLC Genomics Workbench 5.0 software (CLC, Aahus, Denmark). Somatic calling of lymphoblastic tumors and irradiated controls was done using the combined sequence from the three non-irradiated wild type mice as normal control. Only high quality called variants with a minimum 10%

allele frequency and a total read coverage of ten were considered for further analysis. All synonymous variants or variants in non-coding regions except those affecting canonical splice sites were discarded. Remaining variants were assessed manually through the Integrative Genomics Viewer (IGV)[87] for removal of calls due to mapping artifacts or paralogs.

Calling and visualization of copy number alterations was done using the software Control-Free (control-FREE Copy Number Caller) that generates rations from normalized read distribution between tumor and normal followed by visualization in a Shiny application as described previously[105].

RNA sequencing of mouse tumors

Bulk RNA sequencing (RNA-seq) was performed on extracted RNA in a total of 24 samples; 10 controls (thymic tissue from healthy mice) and 14 thymic lymphomas. As with mouse tumor WES, controls were divided into three groups based on irradiation status and genotype: wild-type non-irradiated (n = 3), *PPM1D*-transgenic non-irradiated (n = 3), wild-type irradiated (n = 2), *PPM1D*-transgenic irradiated (n = 2). Total RNA extraction, library preparation and sequencing were performed by Otogenetics (Otogenetics Corporation, Atlanta, GA, USA) through paired-end sequencing on Illumina HiSeq 2500 (Illumina, San Diego, CA) after mRNA purification using the TruSeq Stranded cDNA kit. Read length was 100-125 bp for all samples.

Samples were aligned to the mm10 reference genome using STAR in 2-pass mode[106]. Aligned reads were quantified using htseq-count[107] and differential gene expression analysis was performed using the R/Bioconductor package DESeq2[108]. After having converted mouse Ensembl gene IDs to human orthologs using the R package *gOrth*, gene set enrichment analysis was performed using the GSEA software from Broad institute[109,110] and the Hallmark collection of gene sets from the Molecular Signatures Database, MSigDB, version 6.2[111].

Statistical analysis

Statistical analyses were done with GraphPad Prism software (GraphPad Software, San Diego, CA). The IC_{50} values (inhibitory concentration 50%) were determined from log concentrations-effect curves using non-linear regression analysis. T test was used to compare means between two groups and for comparison of three or more groups, one-way ANOVA followed by Bonferroni multiple-comparisons post-test were used. Survival analysis was examined with log-rank test and Fisher's test was used to test significance of association between the two categories. Correlations were assessed with Pearson test/Spearman non-parametric test. $P<0.05$ was considered significant and all tests were two-sided. Survival curves were calculated using the Kaplan-Meier method. Regarding statistical methods for genomics and transcriptomics studies, please refer to the corresponding methods section.

References

1. Huether, R. *et al*. The landscape of somatic mutations in epigenetic regulators across 1,000 paediatric cancer genomes. *Nat Commun* **5**, 3630 (2014).

2. Downing, J.R. *et al*. The Pediatric Cancer Genome Project. *Nat Genet* **44**, 619-22 (2012).

3. Grobner, S.N. *et al*. The landscape of genomic alterations across childhood cancers. *Nature* **555**, 321-327 (2018).

4. Carr-Wilkinson, J. *et al*. High Frequency of p53/MDM2/p14ARF Pathway Abnormalities in Relapsed Neuroblastoma. *Clin Cancer Res* **16**, 1108-18 (2010).

5. Bown, N. *et al*. Gain of chromosome arm 17q and adverse outcome in patients with neuroblastoma. *N Engl J Med* **340**, 1954-61 (1999).

6. Caren, H. *et al*. High-risk neuroblastoma tumors with 11q-deletion display a poor prognostic, chromosome instability phenotype with later onset. *Proc Natl Acad Sci U S A* **107**, 4323-8 (2010).

7. Saito-Ohara, F. *et al*. PPM1D is a potential target for 17q gain in neuroblastoma. *Cancer Res* **63**, 1876-83 (2003).

8. Fiscella, M. *et al*. Wip1, a novel human protein phosphatase that is induced in response to ionizing radiation in a p53-dependent manner. *Proc Natl Acad Sci U S A* **94**, 6048-53 (1997).

9. Fujimoto, H. *et al*. Regulation of the antioncogenic Chk2 kinase by the oncogenic Wip1 phosphatase. *Cell Death Differ* **13**, 1170-80 (2006).

10. Lu, X., Nannenga, B. & Donehower, L.A. PPM1D dephosphorylates Chk1 and p53 and abrogates cell cycle checkpoints. *Genes Dev* **19**, 1162-74 (2005).

11. Lu, X., Nguyen, T.A. & Donehower, L.A. Reversal of the ATM/ATR-mediated DNA damage response by the oncogenic phosphatase PPM1D. *Cell Cycle* **4**, 1060-4 (2005).

12. Oliva-Trastoy, M. *et al*. The Wip1 phosphatase (PPM1D) antagonizes activation of the Chk2 tumour suppressor kinase. *Oncogene* **26**, 1449-58 (2007).

13. Shreeram, S. *et al*. Regulation of ATM/p53-dependent suppression of myc-induced lymphomas by Wip1 phosphatase. *J Exp Med* **203**, 2793-9 (2006).

14. Castellino, R.C. *et al*. Medulloblastomas overexpress the p53-inactivating oncogene WIP1/PPM1D. *J Neurooncol* **86**, 245-56 (2008).

15. Fuku, T., Semba, S., Yutori, H. & Yokozaki, H. Increased wild-type p53-induced phosphatase 1 (Wip1 or PPM1D) expression correlated with downregulation of checkpoint kinase 2 in human gastric carcinoma. *Pathol Int* **57**, 566-71 (2007).

16. Hirasawa, A. *et al*. Association of 17q21-q24 gain in ovarian clear cell adenocarcinomas with poor prognosis and identification of PPM1D and APPBP2 as likely amplification targets. *Clin Cancer Res* **9**, 1995-2004 (2003).

17. Lambros, M.B. *et al*. PPM1D gene amplification and overexpression in breast cancer: a qRT-PCR and chromogenic in situ hybridization study. *Mod Pathol* **23**, 1334-45 (2010).

18. Nikbakht, H. *et al*. Spatial and temporal homogeneity of driver mutations in diffuse intrinsic pontine glioma. *Nat Commun* **7**, 11185 (2016).

19. Ruark, E. *et al*. Mosaic PPM1D mutations are associated with predisposition to breast and ovarian cancer. *Nature* **493**, 406-10 (2013).

20. Tan, D.S. *et al*. PPM1D is a potential therapeutic target in ovarian clear cell carcinomas. *Clin Cancer Res* **15**, 2269-80 (2009).

21. Zhang, Y. *et al*. WIP1 regulates the proliferation and invasion of nasopharyngeal carcinoma in vitro. *Tumour Biol* **35**, 7651-7 (2014).

22. Karlsson, J. *et al*. Four evolutionary trajectories underlie genetic intratumoral variation in childhood cancer. *Nat Genet* **50**, 944-950 (2018).

23. Krona, C. *et al*. Analysis of neuroblastoma tumour progression; loss of PHOX2B on 4p13 and 17q gain are early events in neuroblastoma tumourigenesis. *Int J Oncol* **32**, 575-83 (2008).

24. Jansen, S. *et al*. De Novo Truncating Mutations in the Last and Penultimate Exons of PPM1D Cause an Intellectual Disability Syndrome. *Am J Hum Genet* **100**, 650-658 (2017).

25. Lelieveld, S.H. *et al*. Meta-analysis of 2,104 trios provides support for 10 new genes for intellectual disability. *Nat Neurosci* **19**, 1194-6 (2016).

26. Cohn, S.L. *et al*. The International Neuroblastoma Risk Group (INRG) classification system: an INRG Task Force report. *J Clin Oncol* **27**, 289-97 (2009).

27. Brodeur, G.M. Neuroblastoma: biological insights into a clinical enigma. *Nat Rev Cancer* **3**, 203-16 (2003).

28. McArdle, L. *et al*. Oligonucleotide microarray analysis of gene expression in neuroblastoma displaying loss of chromosome 11q. *Carcinogenesis* **25**, 1599-609 (2004).

29. Wilzen, A. *et al*. The Phox2 pathway is differentially expressed in neuroblastoma tumors, but no mutations were found in the candidate tumor suppressor gene PHOX2A. *Int J Oncol* **34**, 697-705 (2009).

30. Northcott, P.A. *et al*. Medulloblastoma. *Nat Rev Dis Primers* **5**, 11 (2019).

31. Buss, M.C. *et al*. The WIP1 oncogene promotes progression and invasion of aggressive medulloblastoma variants. *Oncogene* **34**, 1126-40 (2015).

32. Kool, M. *et al*. Genome sequencing of SHH medulloblastoma predicts genotype-related response to smoothened inhibition. *Cancer Cell* **25**, 393-405 (2014).

33. Zhang, X. *et al*. Oncogenic Wip1 phosphatase is inhibited by miR-16 in the DNA damage signaling pathway. *Cancer Res* **70**, 7176-86 (2010).

34. Kryh, H. *et al*. Comprehensive SNP array study of frequently used neuroblastoma cell lines; copy neutral loss of heterozygosity is common in the cell lines but uncommon in primary tumors. *BMC Genomics* **12**, 443 (2011).

35. Schleiermacher, G. *et al*. Variety and complexity of chromosome 17 translocations in neuroblastoma. *Genes Chromosomes Cancer* **39**, 143-50 (2004).

36. Aguirre, A.J. *et al*. Genomic Copy Number Dictates a Gene-Independent Cell Response to CRISPR/Cas9 Targeting. *Cancer Discov* **6**, 914-29 (2016).

37. Armstrong, J.F., Kaufman, M.H., Harrison, D.J. & Clarke, A.R. High-frequency developmental abnormalities in p53-deficient mice. *Curr Biol* **5**, 931-6 (1995).

38. Donehower, L.A. *et al*. Mice deficient for p53 are developmentally normal but susceptible to spontaneous tumours. *Nature* **356**, 215-21 (1992).

39. Jacks, T. *et al*. Tumor spectrum analysis in p53-mutant mice. *Curr Biol* **4**, 1-7 (1994).

40. Mao, J.H. *et al*. Genomic instability in radiation-induced mouse lymphoma from p53 heterozygous mice. *Oncogene* **24**, 7924-34 (2005).

41. Kozakai, Y. *et al*. Inhibition of C-terminal truncated PPM1D enhances the effect of doxorubicin on cell viability in human colorectal carcinoma cell line. *Bioorg Med Chem Lett* **24**, 5593-5596 (2014).

42. Ogasawara, S. *et al*. Novel inhibitors targeting PPM1D phosphatase potently suppress cancer cell proliferation. *Bioorg Med Chem* **23**, 6246-9 (2015).

43. Rayter, S. *et al*. A chemical inhibitor of PPM1D that selectively kills cells overexpressing PPM1D. *Oncogene* **27**, 1036-44 (2008).

44. Yagi, H. *et al*. A small molecule inhibitor of p53-inducible protein phosphatase PPM1D. *Bioorg Med Chem Lett* **22**, 729-32 (2012).

45. Northcott, P.A. *et al*. Enhancer hijacking activates GFI1 family oncogenes in medulloblastoma. *Nature* **511**, 428-34 (2014).

46. Bouska, A. *et al*. Genome-wide copy-number analyses reveal genomic abnormalities involved in transformation of follicular lymphoma. *Blood* **123**, 1681-90 (2014).

47. Carless, M.A. & Griffiths, L.R. Cytogenetics of melanoma and nonmelanoma skin cancer. *Adv Exp Med Biol* **810**, 160-81 (2014).

48. Herou, E., Biloglav, A., Johansson, B. & Paulsson, K. Partial 17q gain resulting from isochromosomes, unbalanced translocations and complex rearrangements is associated with gene overexpression, older age and shorter overall survival in high hyperdiploid childhood acute lymphoblastic leukemia. *Leukemia* **27**, 493-6 (2013).

49. Malouf, G.G. *et al*. Genomic heterogeneity of translocation renal cell carcinoma. *Clin Cancer Res* **19**, 4673-84 (2013).

50. Sunpaweravong, P., Thu, K.L., Lam, W.L. & Mai, S. Assessment of the clinical relevance of 17q25.3 copy number and three-dimensional telomere organization in non-small lung cancer patients. *J Cancer Res Clin Oncol* **142**, 749-56 (2016).

51. Xiang, D.B. *et al*. Molecular cytogenetic characterization of mammary neuroendocrine carcinoma. *Hum Pathol* **45**, 1951-6 (2014).

52. Kleiblova, P. *et al*. Gain-of-function mutations of PPM1D/Wip1 impair the p53-dependent G1 checkpoint. *J Cell Biol* **201**, 511-21 (2013).

53. Tedaldi, G. *et al*. Multiple-gene panel analysis in a case series of 255 women with hereditary breast and ovarian cancer. *Oncotarget* **8**, 47064-47075 (2017).

54. Abdel-Aziz, A., Mohamed, M.A., Akl, F.M. & Taha, A.N. Survivin expression in medulloblastoma: a possible marker for survival. *Pathol Oncol Res* **19**, 413-9 (2013).

55. Adida, C., Berrebi, D., Peuchmaur, M., Reyes-Mugica, M. & Altieri, D.C. Anti-apoptosis gene, survivin, and prognosis of neuroblastoma. *Lancet* **351**, 882-3 (1998).

56. Faccion, R.S. *et al*. Lack of prognostic significance of survivin in pediatric medulloblastoma. *Pathol Oncol Res* **17**, 899-908 (2011).

57. Islam, A. *et al*. High expression of Survivin, mapped to 17q25, is significantly associated with poor prognostic factors and promotes cell survival in human neuroblastoma. *Oncogene* **19**, 617-23 (2000).

58. Artomov, M., Rivas, M.A., Genovese, G. & Daly, M.J. Mosaic mutations in blood DNA sequence are associated with solid tumor cancers. *NPJ Genom Med* **2**, 22 (2017).

59. Krauthammer, M. *et al*. Exome sequencing identifies recurrent somatic RAC1 mutations in melanoma. *Nat Genet* **44**, 1006-14 (2012).

60. Chuman, Y. *et al*. PPM1D430, a novel alternative splicing variant of the human PPM1D, can dephosphorylate p53 and exhibits specific tissue expression. *J Biochem* **145**, 1-12 (2009).

61. Richter, M. *et al*. WIP1 phosphatase as a potential therapeutic target in neuroblastoma. *PLoS One* **10**, e0115635 (2015).

62. Wen, J. *et al*. WIP1 modulates responsiveness to Sonic Hedgehog signaling in neuronal precursor cells and medulloblastoma. *Oncogene* **35**, 5552-5564 (2016).

63. Shiloh, Y. ATM and related protein kinases: safeguarding genome integrity. *Nat Rev Cancer* **3**, 155-68 (2003).

64. Uyanik, B., Grigorash, B.B., Goloudina, A.R. & Demidov, O.N. DNA damage-induced phosphatase Wip1 in regulation of hematopoiesis, immune system and inflammation. *Cell Death Discov* **3**, 17018 (2017).

65. Matthay, K.K. *et al*. Neuroblastoma. *Nat Rev Dis Primers* **2**, 16078 (2016).

66. Chesler, L. *et al*. Chemotherapy-induced apoptosis in a transgenic model of neuroblastoma proceeds through p53 induction. *Neoplasia* **10**, 1268-74 (2008).

67. Weiss, W.A., Aldape, K., Mohapatra, G., Feuerstein, B.G. & Bishop, J.M. Targeted expression of MYCN causes neuroblastoma in transgenic mice. *EMBO J* **16**, 2985-95 (1997).

68. Kratz, C.P. *et al*. Cancer Screening Recommendations for Individuals with Li-Fraumeni Syndrome. *Clin Cancer Res* **23**, e38-e45 (2017).

69. Frank, A.J. *et al*. The TP53-ARF tumor suppressor pathway is frequently disrupted in large/cell anaplastic medulloblastoma. *Brain Res Mol Brain Res* **121**, 137-40 (2004).

70. Zhukova, N. *et al*. Subgroup-specific prognostic implications of TP53 mutation in medulloblastoma. *J Clin Oncol* **31**, 2927-35 (2013).

71. Tong, C.Y. *et al*. Detection of oncogene amplifications in medulloblastomas by comparative genomic hybridization and array-based comparative genomic hybridization. *J Neurosurg* **100**, 187-93 (2004).

1209 72. Kamihara, J. *et al*. Retinoblastoma and Neuroblastoma Predisposition and Surveillance. *Clin*
1210 *Cancer Res* **23**, e98-e106 (2017).

1211 73. Seidinger, A.L. *et al*. Occurrence of Neuroblastoma among TP53 p.R337H Carriers. *PLoS One*
1212 **10**, e0140356 (2015).

1213 74. Ackermann, S. *et al*. A mechanistic classification of clinical phenotypes in neuroblastoma.
1214 *Science* **362**, 1165-1170 (2018).

1215 75. Keshelava, N. *et al*. Loss of p53 function confers high-level multidrug resistance in
1216 neuroblastoma cell lines. *Cancer Res* **61**, 6185-93 (2001).

1217 76. Tweddle, D.A., Malcolm, A.J., Bown, N., Pearson, A.D. & Lunec, J. Evidence for the
1218 development of p53 mutations after cytotoxic therapy in a neuroblastoma cell line. *Cancer Res* **61**, 8-13 (2001).

1219 77. Carr, J. *et al*. Increased frequency of aberrations in the p53/MDM2/p14(ARF) pathway in
1220 neuroblastoma cell lines established at relapse. *Cancer Res* **66**, 2138-45 (2006).

1221 78. Chen, Z. *et al*. Mdm2 deficiency suppresses MYCN-Driven neuroblastoma tumorigenesis in
1222 vivo. *Neoplasia* **11**, 753-62 (2009).

1223 79. Swarbrick, A. *et al*. miR-380-5p represses p53 to control cellular survival and is associated with
1224 poor outcome in MYCN-amplified neuroblastoma. *Nat Med* **16**, 1134-40 (2010).

1225 80. Veschi, V. & Thiele, C.J. High-SETD8 inactivates p53 in neuroblastoma. *Oncoscience* **4**, 21-22
1226 (2017).

1227 81. Bulavin, D.V. *et al*. Inactivation of the Wip1 phosphatase inhibits mammary tumorigenesis
1228 through p38 MAPK-mediated activation of the p16(Ink4a)-p19(Arf) pathway. *Nat Genet* **36**, 343-50 (2004).

1229 82. Liao, M.J. *et al*. No requirement for V(D)J recombination in p53-deficient thymic lymphoma.
1230 *Mol Cell Biol* **18**, 3495-501 (1998).

1231 83. Okazaki, R. & Ootsuyama, A. p53-dependent delayed effects of radiation vary according to time
1232 of irradiation of p53 + / - mice. *J Radiat Res* **55**, 25-31 (2014).

1233 84. Soussi, T. & Lozano, G. p53 mutation heterogeneity in cancer. *Biochem Biophys Res Commun*
1234 **331**, 834-42 (2005).

1235 85. Goh, A.M., Coffill, C.R. & Lane, D.P. The role of mutant p53 in human cancer. *J Pathol* **223**,
1236 116-26 (2011).

1237 86. Caren, H. *et al*. High-resolution array copy number analyses for detection of deletion, gain,
1238 amplification and copy-neutral LOH in primary neuroblastoma tumors: four cases of homozygous deletions of
1239 the CDKN2A gene. *BMC Genomics* **9**, 353 (2008).

1240 87. Robinson, J.T. *et al*. Integrative genomics viewer. *Nat Biotechnol* **29**, 24-6 (2011).

1241 88. Pharoah, P.D.P. *et al*. PPM1D Mosaic Truncating Variants in Ovarian Cancer Cases May Be
1242 Treatment-Related Somatic Mutations. *J Natl Cancer Inst* **108**(2016).

1243 89. Zhang, W. *et al*. Comparison of RNA-seq and microarray-based models for clinical endpoint
1244 prediction. *Genome Biol* **16**, 133 (2015).

90. Brodeur, G.M. *et al*. Revisions of the international criteria for neuroblastoma diagnosis, staging, and response to treatment. *J Clin Oncol* **11**, 1466-77 (1993).

91. Theissen, J. *et al*. Chromosome 17/17q gain and unaltered profiles in high resolution array-CGH are prognostically informative in neuroblastoma. *Genes Chromosomes Cancer* **53**, 639-49 (2014).

92. Hothorn, T.L., B. On the exact distribution of maximally selected rank statistics. *Computational Statistics & Data Analysis* **43**, 121-137 (2003).

93. R-Core-Team. R: A language and environment for statistical computing. *Vienna, Austria: R Foundation for Statistical Computing* (2013).

94. Abel, F. *et al*. A 6-gene signature identifies four molecular subgroups of neuroblastoma. *Cancer Cell Int* **11**, 9 (2011).

95. Birks, D.K. *et al*. High expression of BMP pathway genes distinguishes a subset of atypical teratoid/rhabdoid tumors associated with shorter survival. *Neuro Oncol* **13**, 1296-307 (2011).

96. Fattet, S. *et al*. Beta-catenin status in paediatric medulloblastomas: correlation of immunohistochemical expression with mutational status, genetic profiles, and clinical characteristics. *J Pathol* **218**, 86-94 (2009).

97. Kool, M. *et al*. Integrated genomics identifies five medulloblastoma subtypes with distinct genetic profiles, pathway signatures and clinicopathological features. *PLoS One* **3**, e3088 (2008).

98. Robinson, G. *et al*. Novel mutations target distinct subgroups of medulloblastoma. *Nature* **488**, 43-8 (2012).

99. Roth, R.B. *et al*. Gene expression analyses reveal molecular relationships among 20 regions of the human CNS. *Neurogenetics* **7**, 67-80 (2006).

100. Lindhagen, E., Nygren, P. & Larsson, R. The fluorometric microculture cytotoxicity assay. *Nat Protoc* **3**, 1364-9 (2008).

101. Gallo-Oller, G. *et al*. P144, a Transforming Growth Factor beta inhibitor peptide, generates antitumoral effects and modifies SMAD7 and SKI levels in human glioblastoma cell lines. *Cancer Lett* **381**, 67-75 (2016).

102. Meyers, R.M. *et al*. Computational correction of copy number effect improves specificity of CRISPR-Cas9 essentiality screens in cancer cells. *Nat Genet* **49**, 1779-1784 (2017).

103. Szklarczyk, D. *et al*. The STRING database in 2017: quality-controlled protein-protein association networks, made broadly accessible. *Nucleic Acids Res* **45**, D362-D368 (2017).

104. Sveinbjornsson, B. *et al*. Expression of enzymes and receptors of the leukotriene pathway in human neuroblastoma promotes tumor survival and provides a target for therapy. *FASEB J* **22**, 3525-36 (2008).

105. Fransson, S. *et al*. Estimation of copy number aberrations: Comparison of exome sequencing data with SNP microarrays identifies homozygous deletions of 19q13.2 and CIC in neuroblastoma. *Int J Oncol* **48**, 1103-16 (2016).

106. Dobin, A. *et al*. STAR: ultrafast universal RNA-seq aligner. *Bioinformatics* **29**, 15-21 (2013).

107. Anders, S., Pyl, P.T. & Huber, W. HTSeq--a Python framework to work with high-throughput sequencing data. *Bioinformatics* **31**, 166-9 (2015).

108. Love, M.I., Huber, W. & Anders, S. Moderated estimation of fold change and dispersion for RNA-seq data with DESeq2. *Genome Biol* **15**, 550 (2014).

109. Mootha, V.K. *et al*. PGC-1alpha-responsive genes involved in oxidative phosphorylation are coordinately downregulated in human diabetes. *Nat Genet* **34**, 267-73 (2003).

110. Subramanian, A. *et al*. Gene set enrichment analysis: a knowledge-based approach for interpreting genome-wide expression profiles. *Proc Natl Acad Sci U S A* **102**, 15545-50 (2005).

111. Liberzon, A. *et al*. The Molecular Signatures Database (MSigDB) hallmark gene set collection. *Cell Syst* **1**, 417-425 (2015).

Figures outline

1. Fig 1A-F
2. Fig 2A-C
3. Fig 3A-K
4. Fig 4A-D
5. Fig 5A-F
6. Fig 6A-E

Figure 1

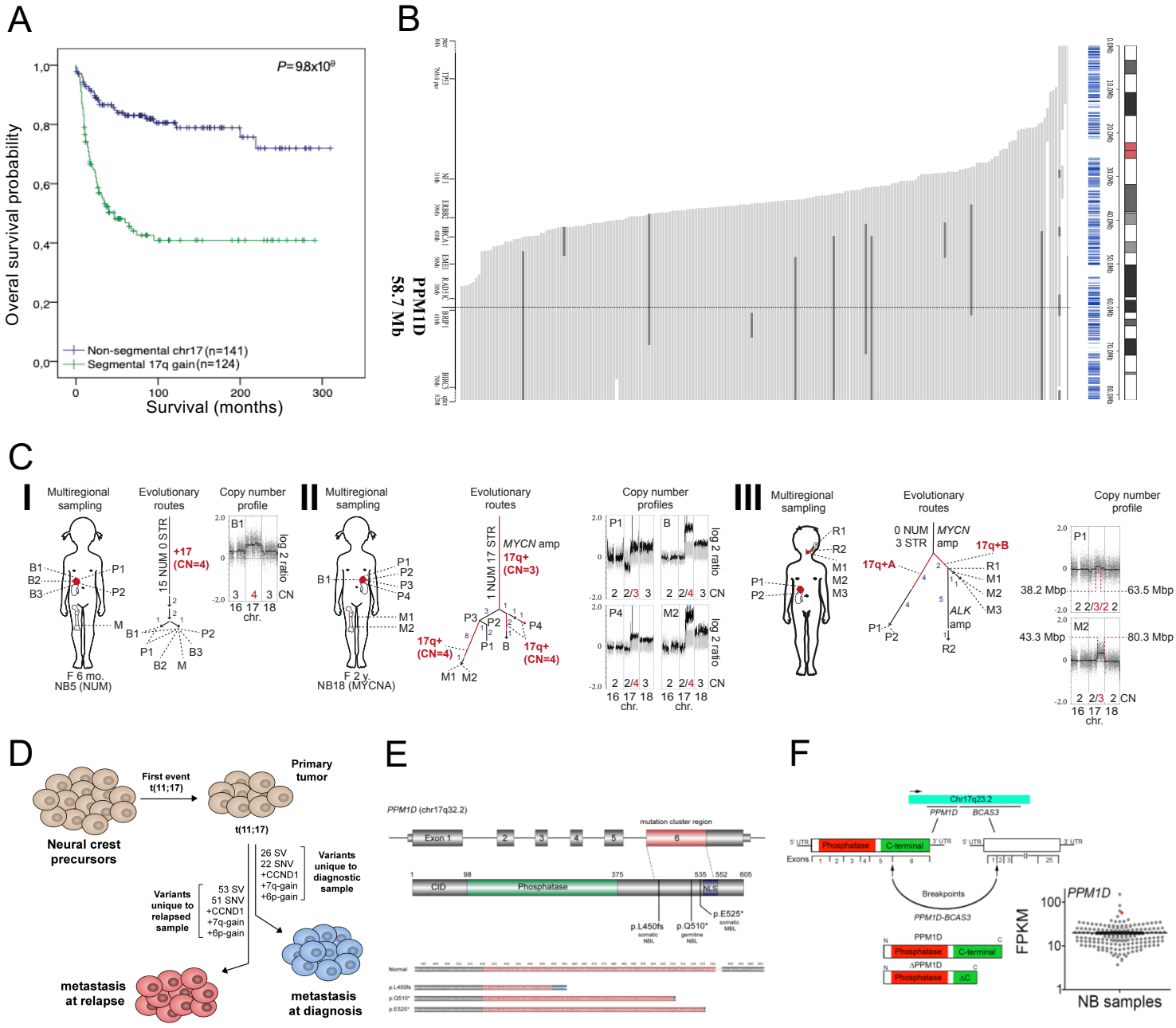

Figure 1. The *PPM1D* gene located on chromosome 17q is frequently altered in neuroblastoma. A. Gain of 17q correlates with poor survival in neuroblastoma. Neuroblastoma survival probability according to Kaplan-Meier analysis in a Swedish population-based patient material in relation to chromosome 17 status in the tumor tissue shows worse overall survival (OS) for children with 17q segmental gain (n=124; green line, 48.0% 5 year OS) vs children with no segmental 17q gain (n=141; blue line, 82.8% 5 year OS). For definition of the genomic profile groups (*Carén et al. 2010*). **B.** *PPM1D* is included in all cases of 17q gain. Summary of segmental gains of chromosome 17 in the extended Swedish neuroblastoma cohort (n=435). 208 samples displayed segmental gain of chromosome 17 as indicated by gray horizontal bars with regions displaying additional level of gain (more copies) indicated by black color. The dotted vertical line indicates location of the *PPM1D* locus in relation to the segmental 17q gains in the cohort. An additional 149 cases showed whole chromosome gain of chromosome 17 (not shown in the figure). **C.** Evolutionary trajectories of PPM1D gain. Multiregional tumor sampling reveals *PPM1D* copy number accumulation in high risk neuroblastoma. **(I)** Genome array analysis of pre-treatment biopsies (B1-B3), post-chemotherapy resection specimens (P1-P2) and concurrent bone marrow metastasis (M) from a female (F) 6-month-old (mo.) patient with a low risk neuroblastoma (NB), having a whole genome profile with only numerical (NUM) changes (I, left). Evolutionary reconstruction (I, center) shows 15 aberrations in the phylogenetic stem, i.e. present in >90% of tumor cells in all samples, followed by several additional whole chromosome changes at subclonal levels (arrows with numbers in blue type), distributed over a subset of samples. The stem aberrations include four copies (CN=4) of chromosome 17, as shown by a higher log2 ratio (I, right) than for the trisomic chromosomes (chr. 16 and 18).

2

Figure 1

No further chromosome 17 aberrations were detected. **(II)** Multiregional array analysis of a *MYCN* amplified (MYCNA) high-risk NB in a 2-year-old (y.) with a metastatic relapse in the bone marrow indicates a stem dominated by structural (STR) rearrangements including segmental gain (CN=3) of the *PPM1D* region in 17q. Additional *PPM1D*/17q copies (CN=4) are gained in samples B, M1, M2 and P4 either clonally (>90% of tumor cells, red line) or subclonally (red arrow). **(III)** Another high-risk *MYCN* amplified NB demonstrates parallel evolution of *PPM1D*/17q gain in different tumor regions, as evidenced by different genomic breakpoints (III, right) in different sample sets, including two temporally distinct relapses (R1 and R2). **D.** Gain of 17q including PPM1D is the first and only common aberration in a high-risk metastatic neuroblastoma. Whole genome sequencing of different metastatic sites at diagnosis and relapse revealed an unbalanced translocation t(11;17) as the only common aberration whereas multiple unique but different genetic aberrations unique to respective sample were present in the two metastatic clones sequenced. **E.** Schematic representation of coding and protein sequence of *PPM1D*/WIP1 with mutations shown according location in protein and predicted amino acid sequences resulting from the *PPM1D* variants detected in neuroblastoma (NBL) and medulloblastoma (MBL) patients. Amino acids translated from exon 6 depicted in red with mutated amino acids depicted in blue. **F.** *PPM1D* expression levels are high in neuroblastoma tumor (red) bearing transcript of the *PPM1D–BCAS3* fusion, shown by FPKM (Fragments Per Kilobase per Million mapped reads).

Figure 2

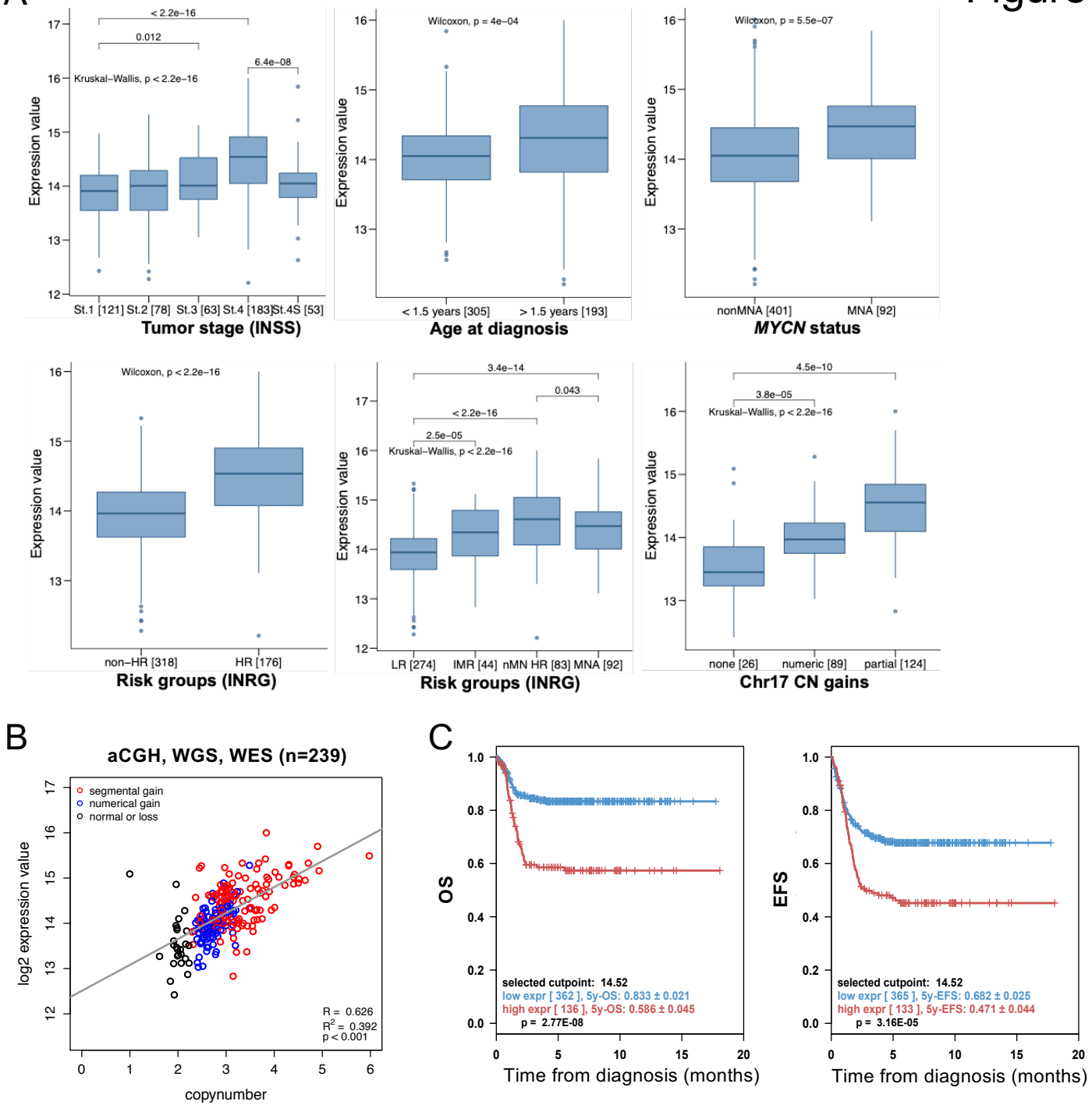

Figure 2. *PPM1D* expression correlates with unfavorable prognosis markers, decreased survival of neuroblastoma patients, and is gene-dosage dependent. **A.** Expression of *PPM1D* is associated with unfavorable prognostic markers. *PPM1D* expression is shown in box-and whisker plots for neuroblastoma tumor stages according to the INSS classification, age at diagnosis, amplification status of *MYCN*, INRG risk group classification (LR=low risk, IMR= intermediate risk, NMN HR= non-*MYCN* amplified high risk, MNA=*MYCN* amplified), and chromosome 17 copy number (CN) gains. **B.** Correlation analysis showing a gene-dosage dependent expression pattern of *PPM1D*. Quantitative copy number information for *PPM1D* based on CGH, whole exome (WES) and whole genome sequencing (WGS) data (x-axis) is shown against normalized log2 expression values from paired RNA-Seq data (y-axis). CN gains are highlighted and separated into numerical gains copying the whole chromosome 17 (blue) and segmental gains affecting only a sub-region involving *PPM1D* (red, min/max/mean size 2.4/70.8/35.8 Mb). Correlation and P-values were obtained by Pearson's correlation coefficient. **C.** High expression of *PPM1D* is associated with adverse patient outcome. Kaplan–Meier survival estimates are shown for overall survival (OS, left) and event-free survival (EFS, right) in the whole cohort (n=498). P values were obtained by log-rank test. The cohort was dichotomized according to the optimal cut-off expression for *PPM1D*.

Figure 3

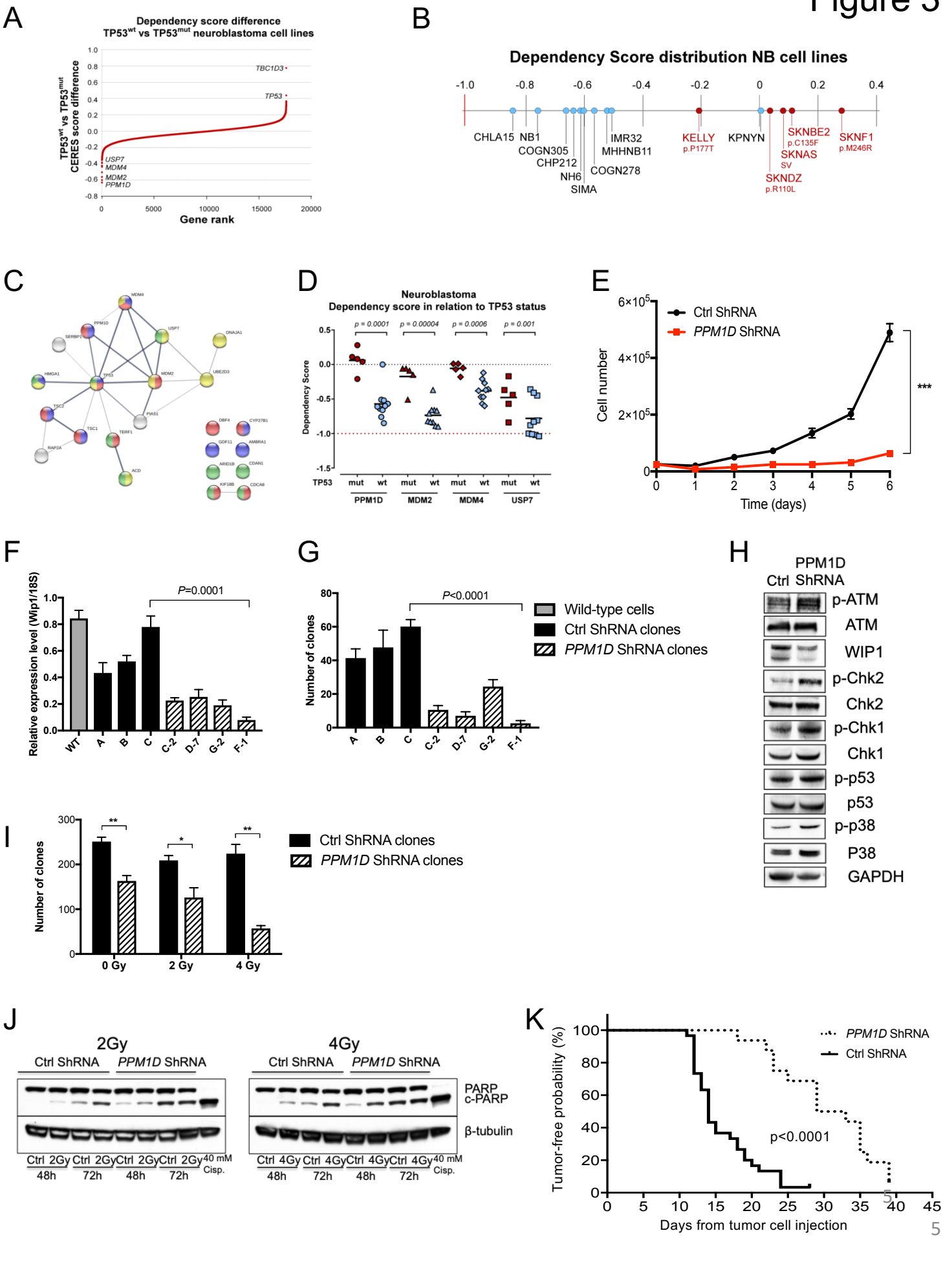

Figure 3

Figure 3. *PPM1D* expression is important for neuroblastoma **A.** Wild type *TP53* neuroblastoma cells are highly dependent on *PPM1D* expression for survival. Genome-scale CRISPR-Cas9 screening showing ranked average difference in genetic dependencies between wild- type *TP53* and mutated *TP53* neuroblastoma cell lines. **B.** Dependency score showing high *PPM1D* dependency in wild-type *TP53* neuroblastoma cells. Wild-type *TP53* neuroblastoma cell lines (blue, high dependency) and *TP53* mutated cell lines (red, low dependency) with *TP53* status. **C.** STRING database analysis showing *PPM1D* dependency in wild-type TP53 neuroblastoma cells. Among the top 30 genes with largest different in CERES score there was enrichment of genes involved in negative regulation of cell proliferation (indicated in blue), cell cycle process (red), cellular response to DNA damage (yellow) and chromosome organization (green). The width of the edges corresponds to level of confidence (medium confidence STRING scores of 0.4; high confidence STRING score 0.7; and highest confidence STRING score 0.9). **D.** Neuroblastoma cells with wild-type *TP53* are dependent on *PPM1D* expression for survival. Dependency scores of *PPM1D, MDM2, MDM4*, and *USP7* in relation to *TP53* mutational status. **E.** Knockdown of *PPM1D* with shRNA impairs growth of neuroblastoma cell line SK-N-BE(2). Mean with S.D. of three independent experiments are shown (t-test day 6, SK-N-BE(2) P=0.0002. **F.** ShRNA-mediated knockdown of *PPM1D*. Normalized *PPM1D* mRNA expression in wild-type SK-N-BE(2) cells (grey bar) compared to three clones transfected with a non-silencing control shRNA (black bars, A, B, C) and four different *PPM1D* shRNA knockdown clones (hatched bars, C-2, D-7, G-2 and F-1). The expression of *PPM1D* mRNA was significantly lower in the clones transfected with the different *PPM1D* shRNAs compared to the control transfected clones (one-way ANOVA with Bonferroni correction P<0.05). Mean with S.D. of three determinants are shown. **G.** Knockdown of *PPM1D* inhibits colony-forming potential of neuroblastoma cells. Clonogenic assay of SK-N-BE(2) cells showing decreased colony formation in shRNA *PPM1D* knockdown cells (one-way ANOVA with Bonferroni post test P<0.0001) with lowest colony forming ability in the F-1 clone (t-test. P<0.0001). Mean with S.D. of nine determinants are displayed. **H.** Knockdown of *PPM1D* inhibits dephosphorylation of WIP1 target genes. Phosphorylation levels of WIP1 targets increased after *PPM1D* knockdown (clone F-1) compared to control transfected cells (clone C), as shown by western blotting. **I.** *PPM1D* downregulation sensitizes neuroblastoma cells to irradiation. *PPM1D* knockdown of SK-N-BE(2) cells showed an irradiation dose-dependent decrease in clonogenic forming ability compared to control transfected cells. Mean with S.D of three experiments are displayed (t-test, 0 Gy P=0.00486, 2 Gy P=0.0277, 4 Gy P=0.0015). **J.** ShRNA-mediated knockdown of *PPM1D* increases irradiation-induced apoptosis. Protein expression of the pro-apoptotic marker cPARP in *PPM1D* knockdown cells compared to control transfected cells 48 and 72 hours after exposure to irradiation, analyzed by western blot. β-tubulin was used as protein loading control. **K.** Knockdown of *PPM1D* delays neuroblastoma development. Clone F-1 and control clone C were injected in NMRI *nu/nu* mice (shRNA; n=8, control; n=15), 5 million cells sc. bilaterally. Tumor development was significantly delayed (log-rank test P<0.0001) showing median tumor development (0.100 mL) to be more than doubled (33 days median, vs. 15 days) after *PPM1D* downregulation (dashed line) compared to animals injected with cells transfected with the non-silencing control shRNA (black line).

Figure 4

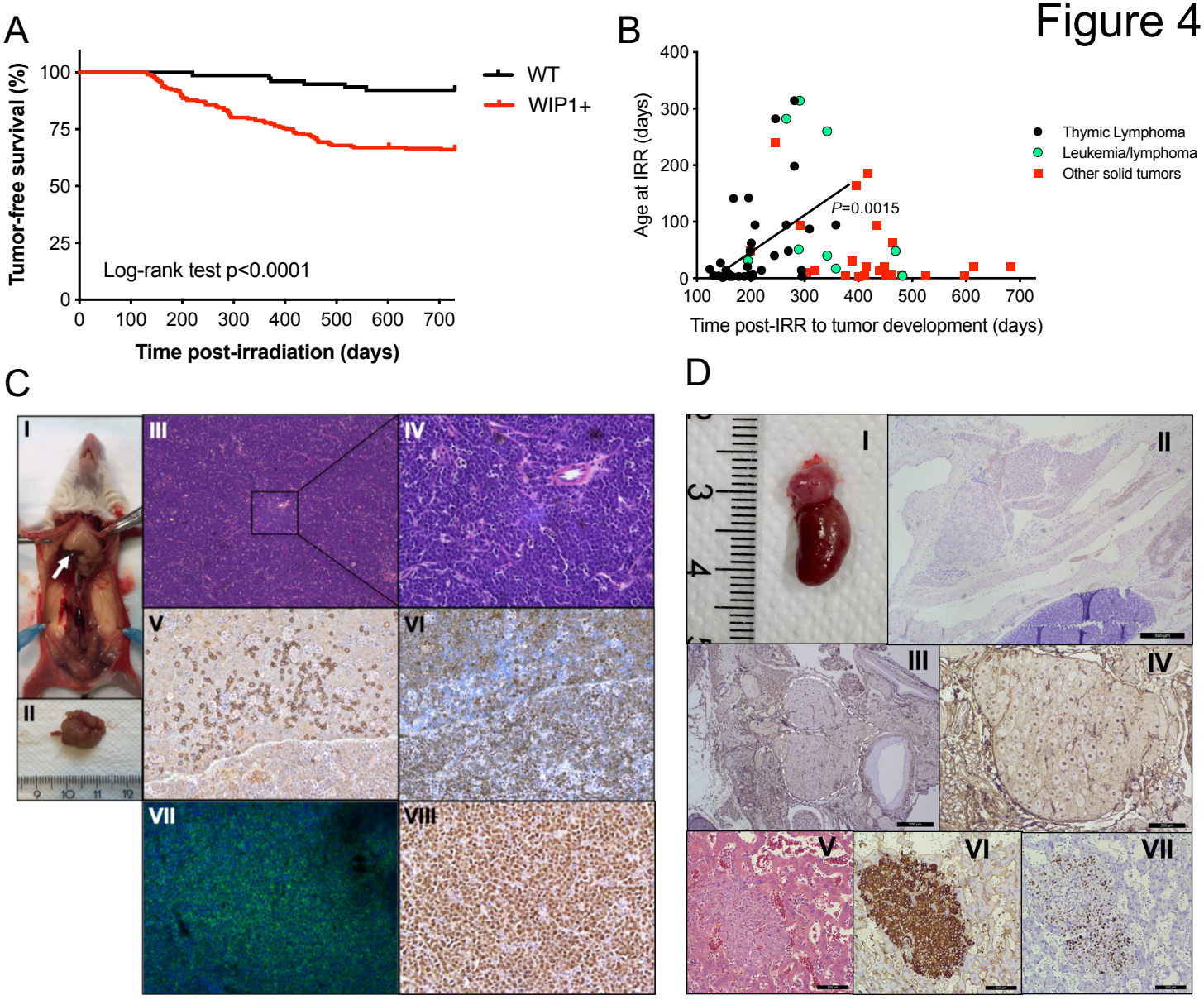

Figure 4. *PPM1D*/WIP1-transgenic mice have increased carcinogenic susceptibility compared to wild-type mice following irradiation. A. Kaplan-Meier analysis of irradiated *PPM1D*/WIP1-transgenic mice with the endpoint defined as detection of tumors. Mice were either homozygous or heterozygous for the human *PPM1D* gene. WIP1 positive transgenic mice (n=210) and their wild-type littermates (n=79) with different degrees of 129X1/SvJ-strain background were subjected to one 4.5 Gy sublethal whole-body irradiation dose at different days of age (1-314 days old). Mice that were positive for the human *PPM1D* gene developed frequently more tumors compared to wild-type mice (Log rank test, $P<0.0001$) following irradiation. Among the *PPM1D*/WIP1-positive mice 72 mice developed tumors compared with six mice in the wild-type group (Fisher's exact test, $P<0.0001$). The odds ratio of developing cancer in the *PPM1D*/WIP1-positive group compared to the wild-type group was 6.3 (95% confidence interval 2.7-14.2). **B.** Time to tumor development of thymic lymphomas post-irradiation (IRR) correlated positively with age at irradiation (Pearson, $P=0.0015$. Spearman, $P=0.001$); the majority of lymphomas manifested <300 days. There was no correlation between age at irradiation and time to tumor development in mice diagnosed with other solid tumors (Pearson $P=0.0658$, Spearman $P=0.1589$) and mice diagnosed having leukemia/lymphoma (Pearson $P=0.3651$, Spearman $P=0.1977$) **C.** Thymic lymphomas were the most common disease manifestation in irradiated human *PPM1D*/WIP1-positive mice**.** Representative image of thoracic tumor *in situ* indicated by the arrow (**I**) and after dissection (**II**). Microscopy at 4X (**III**) and 20X (**IV**) magnification after hematoxylin and eosin (H&E) staining showed atypical lymphoblastic cells having intense mitotic activity. **V)** Infiltration of B220-positive cells. **VI-VII)** The majority of cells are positive for the pan-T cell marker CD3. **VIII**) Staining for Ki-67 was highly positive, indicating high proliferative activity. The thoracic organs, mediastinum (heart base and hilum of the lung), thymus tumor, lymph nodes displayed extensive infiltrates of neoplastic and highly malignant lymphoblasts consistent with lymphoblastic lymphoma. **D.** Adrenal neuroblastic tumor and liver metastasis from a *PPM1D*/WIP1 transgenic mouse **I**) Macroscopic view of the adrenal tumor. **II)** Hematoxylin/Eosin staining of the adrenal tumor. **III-IV)** PHOX2B-staining was positive indicating neural crest origin of this neuroblastoma-like tumor. **V-VII)** Liver metastasis with Hematoxylin/Eosin-staining, Synapotophysin-staining and PHOX2B-staining, respectively.

Figure 5

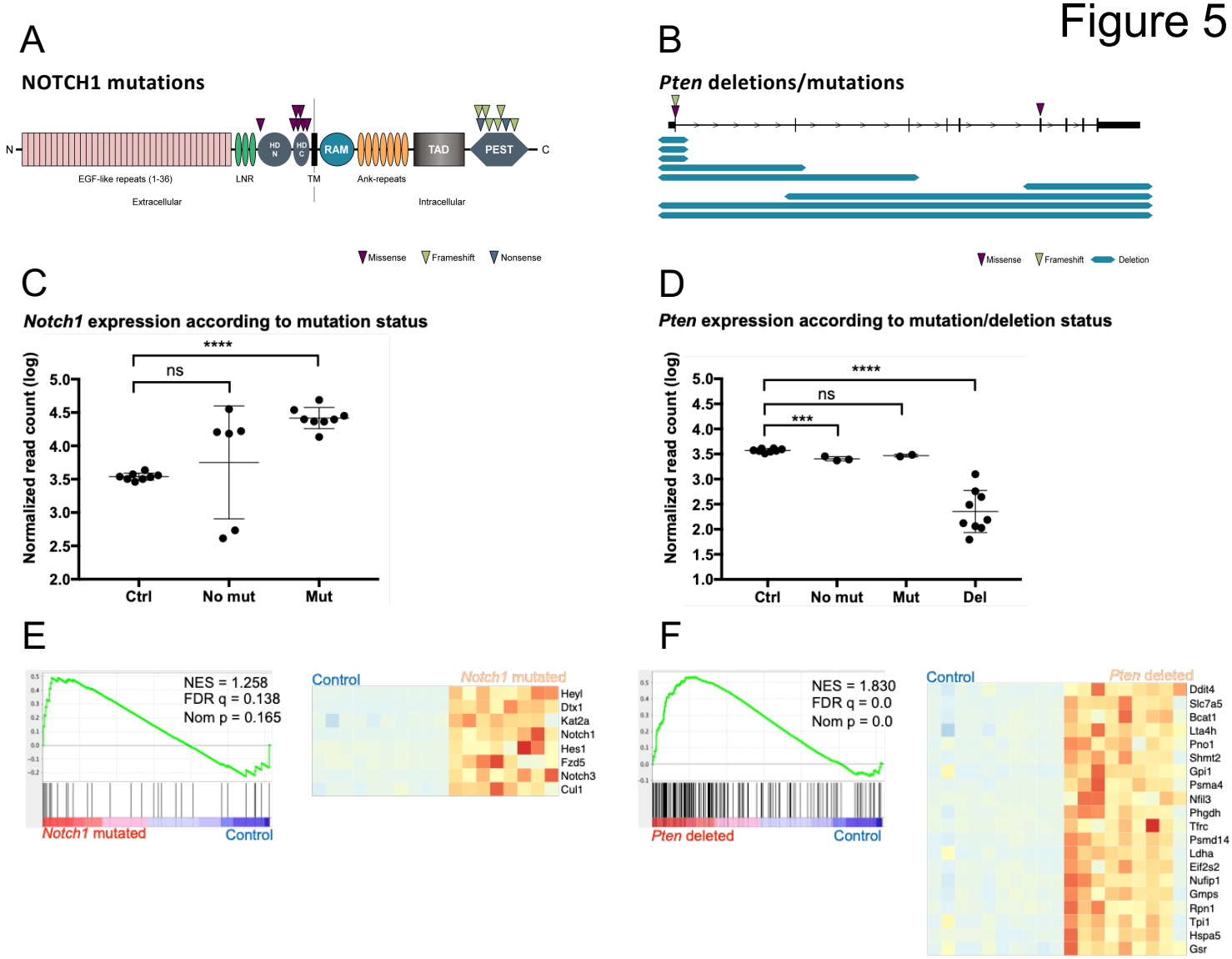

Figure 5. *PPM1D*-induced thymic lymphomas show typical *Notch1* and *Pten* aberrations. A. Schematic overview of the NOTCH1 protein showing the distribution of mutations in 15 whole-exome sequenced lymphomas. Purple triangles indicate missense mutations in the intracellular heterodimerization (HD) domain, whereas green and blue triangles indicate frameshift or nonsense mutations in the extracellular PEST domain. LNR: Lin/NOTCH repeats; HD: heterodimerization domain; TM: transmembrane domain; RAM: RBP-JK associated molecule region; TAD: transactivation domain; PEST: sequence rich in proline, glutamic acid, serine, and threonine. **B.** Diagram of the *Pten* gene showing the size and distribution of *Pten* deletions/mutations in lymphomas. The location of the point mutations are shown with purple and green triangles above the gene diagram. The blue lines below the gene diagram shows the size of the deletions identified by exome sequencing. **C.** Expression of the *Notch1* transcript in controls and tumors with and without *Notch1* mutation. The y axis shows the log value of the number of RNA-seq reads mapping to the *Notch1* gene. The difference between controls and tumors without *Notch1* mutations is not significant (ns), whereas *Notch1* expression is significantly higher in the mutated tumors (adjusted p value < 0.0001; Bonferroni multiple comparisons test). **D.** Expression of *Pten* in controls and tumors with and without *Pten* mutation/deletion. Expression is significantly lower in tumors harboring deletions than in controls (adjusted p value 0,0001, Bonferroni multiple comparisons test). **E.** Gene set enrichment analysis comparing *Notch1* mutated tumors to controls demonstrated a significant upregulation of genes related to Notch signalling (MSigDB ”Hallmarks” gene set). Left panel: Enrichment plot from GSEA. Right panel: Heatmap showing the expression (z scores) of core enriched genes. Red color indicates positive z scores; blue color indicates negative z scores. **F.** Gene set enrichment analysis comparing *Pten* deleted tumors to controls demonstrated upregulation of genes related to the Mtorc1 pathway (MSigDB “Hallmarks” gene set). Left panel: Enrichment plot from GSEA. Right panel: Heatmap showing the expression (z scores) of the top 20 core enriched genes. Red color indicates positive z scores; blue color indicates negative z scores.

Figure 6

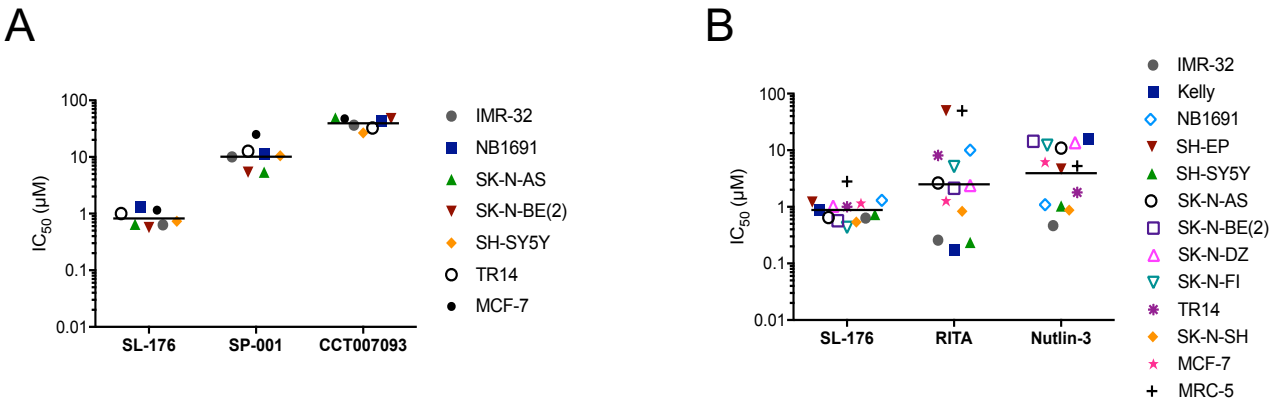

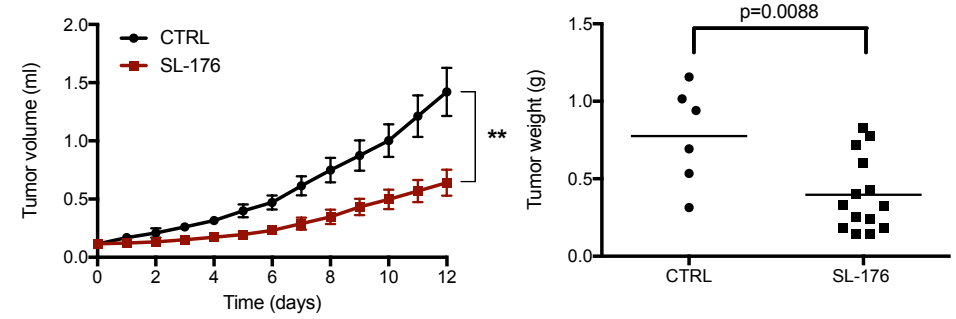

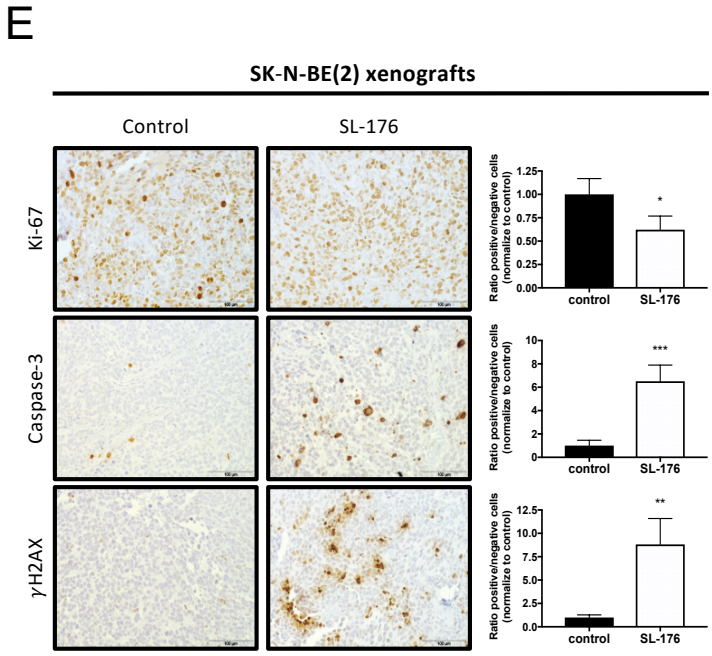

9

Figure 6

Figure 6. The WIP1 phosphatase inhibitor SL-176 suppresses neuroblastoma and medulloblastoma growth *in vitro* and *in vivo*. A. SL-176 is the most efficient inhibitor of tumor cell growth. IC_{50} values for six neuroblastoma cell lines and the *PPM1D*-amplified breast cancer cell line MCF-7 exposed to the WIP1 inhibitors SL-176, SP001 or CCT007093. Horizontal lines indicate mean. IC_{50} values were calculated from cell viability assays performed at least three times. SL-176 displayed the lowest mean of IC_{50} value of the three tested WIP1 inhibitors (one-way ANOVA on log IC50 $P<0.0001$, Bonferroni post-test: SL-176 vs SP-001 $P<0.0001$, SL-176 vs CCT007093 $P<0.0001$). **B**. SL-176 is a potent inhibitor of neuroblastoma cell growth. IC_{50} values for eleven neuroblastoma cell lines, the breast cancer cell line MCF-7 and the fibroblast cell line MRC-5 exposed to the specific WIP1 inhibitor SL-176, the p53-MDM2 interaction inhibitor RITA or the MDM2 antagonist Nutlin-3. Horizontal lines indicate mean. SL-176 displayed the lowest mean of IC_{50}s in the neuroblastoma cell lines of the three tested compounds (mean IC_{50} for SL-176: 0.77 µM, RITA: 2.0 µM and Nutlin-3: 3.7 µM), however a significant difference was only evident between SL-176 and Nutlin-3 (one-way ANOVA $P=0.029$, Bonferroni post-test SL-176 vs. Nutlin-3 $P=0.026$). IC_{50} values were calculated from results from cell viability assay WST-1 performed at least three times. **C.** SL-176 inhibit neuroblastoma growth *in vivo*. Nude mice were injected with neuroblastoma SK-N-BE(2) cells to form xenografts on the flank. Daily i. p. injections of SL-176 (n=14) for 12 days, starting at tumor volume 0.1 mL, compared to no treatment (CTRL, n=6) showed that WIP1 inhibition through SL-176 significantly impaired the growth of neuroblastoma xenografts (t-test, day 12 $P=0.002$) (left, horizontal bars, mean weight), and significantly reduced tumor weight after 12 days ($P=0.0088$) (right). Mean with S.E.M. are displayed. **D.** Representative photograph of dissected neuroblastoma xenograft tumor in comparison. **E.** SL-176 decrease proliferation, induce apoptosis and activate γH2AX in xenograft tumors. Immunohistochemical analysis of SK-N-BE(2) xenograft tumors. Tumor sections were stained with anti-Ki-67, anti-Caspase 3, and anti γH2AX antibodies. Representative examples of immunostaining are shown. Images were acquired at 400X magnification. Identification and quantification of positive and negative cells was carry out with ImageJ software.